ISSN 0036-0236, Russian Journal of Inorganic Chemistry, 2017, Vol. 62, No. 13, pp. 1730–1769. © Pleiades Publishing, Ltd., 2017.

Modeling of Self-Organization Processes in Crystal-Forming Systems: Symmetry and Topology Code for the Cluster Self-Assembly of Crystal Structures of Intermetallic Compounds

G. D. Ilyushin[a, b]

[a] *Shubnikov Institute of Crystallography of Federal Scientific Research Center "Crystallography and Photonics" of Russian Academy of Sciences, Moscow, 119333 Russia*

[b] *Samara Center for Theoretical Materials Science (SCTMS), Samara National Research University, Samara, 443011 Russia*

e-mail: ilyushin@mail.ru

Received May 24, 2017

Abstract—We performed the combinatorial and topological modeling of 1D, 2D, and 3D packs of symmetrically connected metal clusters in the form of tetrahedra A_4. Three types of 1D chains with tetrahedral connectivity of 4, 6, and 8 were used to model 2D layers L-1, L-2, and L-3 and 3D frameworks FR-1, FR-2, FR-3, and FR-4. The model structures of the identified suprapolyhedral precursor clusters were used in topological analysis of crystal structures of intermetallic compounds (program package TOPOS and data bases ICSD and CRYSTMET). A match was found between the topological models of tetrahedral 3D frameworks and all types of crystal structures formed in binary systems; in Au–Cu: FR-1 for Cu_3Au-cP4 (Auricupride), Cu_2Au_2-tP2 (Tetraauricupride), $CuAu_3$-cP4 (Bogdanovite), and $Cu_{2-x}Au_{2+x}$-cF4; in Mg–Cd: FR-3 for Mg_3Cd-hP8, Mg_2Cd_2-oP4, $MgCd_3$-hP8, and $Mg_{2-x}Cd_{2+x}$-hP2; in Li–Hg: FR-2 for Li_3Hg-cF16 and Li_2Hg_2-cP2 and FR-3 for $LiHg_3$-hP8; in ternary system Li–Ag–Al: FR-2 for $LiAg_2Al$-cF16 and Li_2AgAl-cF16; and in quaternary system: framework FR-2 for LiMgPdSn-cF16. Framework FR-4 was identified in ternary intermetallic compounds $A(Li_2Sn_2)$-tI20, where A = Cu, Ag, Au. The structures of precursor nanoclusters were identified for other most abundant types of crystal structures of intermetallic compounds. For this purpose, we used the algorithms for partitioning the structural graph into nonintersecting cluster substructures and constructed the basal 3D network of the crystal structure in the form of a graph whose nodes correspond to the positions of the centers of precursor clusters. The cluster self-assembly was modeled for the following intermetallic compounds: Mg_2Cu_4-cF24, $MgSnCu_4$-cF24, $(ZrCu)Cu_4$-cF24, Mg_2Zn_4-hP12, $(CaCu)Cu_4$-hP6, Cr_3Si-cP8, $Lu_3Co(Fe_3C)$-cP16, $Ca_2Ge_2(Cr_2B_2)$-oC8, $Y_2Ni_2(Fe_2B_2)$-oP8, AlB_2-hP3, Ca_2Ge-oP12, $CaHg_2$-hP3, $Co_2Ge(Ni_2In)$-hP6, Cs_2Hg_4-oI12, Ba_4Po_4-cF8, Mn_5Ge_3-hP16, and $NaZn_{13}$-cF112. The symmetry and topological code of self-assembly from precursor nanoclusters was reconstituted for all crystal structure types of intermetallic compounds as: primary chain → microlayer → microframework. An abundance frequency analysis of topological and symmetry routes for the generation and evolution of precursor clusters enabled us to elucidate the crystal-formation laws in intermetallic systems on the microscopic level.

DOI: 10.1134/S0036023617130046

When studying crystal formation mechanisms, one meets a number of unsolved problems, the solution of which calls for the development of special methods and approaches. These problems can be formulated as follows [1]:

How is the crystallization phenomenon predetermined by the individual geometrical and topological properties of individual particles composing a crystal-forming medium?

What are the universal scenarios (in terms of topology and symmetry) of "disorder–order" kinetic phase transitions in chemically different systems?

How do individual atomic ensembles or polyhedral clusters synergistically interact to provide certain macroscopic spatial characteristics of the system, determining transition from chaos to order through self-organization?

How can one interpret the following sequence of significant elementary events: nanocluster S_3^0—primary chain S_3^1—microlayer S_3^2—microframework S_3^3?

More than 2000 topological types of 3D atomic networks have been classified for more than 27000 crystal structures of intermetallic compounds [2–11]. The distribution of crystal structures of intermetallic compounds among the space groups and the number of representatives among the topological types is dramatically differentiated. For most intermetallic com-

pounds, precursor clusters S_3^0 of crystal structures have not yet been identified. Among those, there are the fifteen most abundant topological types of binary intermetallic compounds A_mB_n, which were determined as long ago as in 1920–1935 and now account to up to one hundred representatives, which is about 60% of the studied intermetallic compounds.

Binary intermetallic compounds typically have composition AB_3, A_2B_2, A_2B_4 (AB_2), or AB_5, cubic or hexagonal symmetry, and high coordination numbers of atoms A and B [2–11]. Presumably, the precursor clusters involved in the self-assembly of typical crystal structures of intermetallic compounds are primarily tetrahedral clusters A_4, octahedral clusters A_6, and icosahedral clusters i-$A_{12}B$. These polyhedra have the greatest number of bonds formed by each atom with neighboring atoms and belong to the family of deltahedra (polyhedra with triangular faces).

Polyhedral metal clusters A_4 and i-$A_{12}B$ are characterized by high-symmetry point groups $-43m$, m-$3m$, and -$3m$ and their subgroups. Statistically, the crystal structures of 60% binary intermetallic compounds (of about 10 000 compounds) are described by eight point groups: $P6_3/mmc$, 13.78%; Fm-$3m$, 13.71%; Pm-$3m$, 7.82%; Im-$3m$, 5.70%; $Pnma$, 5.23%; $I4/mmm$, 4.19%; R-$3m$, 4.19%; and Fd-$3m$, 4.08%). The polyhedral metal clusters A_4, A_6, and i-$A_{12}B$ retain their high symmetry upon crystallization, and this is just responsible for such a limited set of space groups, namely, eight of the 154 for binary intermetallic compounds. For 63% of the ternary intermetallic compounds (out of about 15000 compounds), a limited set of 10 symmetry groups was found (out of 146): Fd-$3i$, 8.59%; $P6_3/mmc$, 8.58%; $I4/mmm$, 8.51%; $P6/mmm$, 7.17%; Fm-$3m$, 6.14%; Pm-$3m$, 5.42%; $Pnma$, 4.97%; $Cmcm$, 4.97%; P-$62m$, 4.35%; and F-$43m$, 4.23%.

We have modeled the crystallographic packing of tetrahedra. Eleven combinatorially possible types of suprapolyhedral clusters with polyhedral connectivity of 1 to 8 have been classified. Primary chains with tetrahedral connectivity of 4, 6, and 8 have been used to model 2D layers and 3D frameworks. Topological types of 3D frameworks have been sought for among the binary, ternary, and quaternary intermetallic compounds (using program package TOPOS [12, 13] and databases ICSD [14] and CRYSTMET [15]). In order to identify precursor nanoclusters in all crystal structures of intermetallic compounds, we have used special algorithms for partitioning the structural graph into nonintersecting cluster substructures and constructed the basal 3D network of the structure in the form of a graph whose nodes correspond to the positions of the centers of precursor clusters. The symmetry and topology code of self-assembly for representative crystal structures of intermetallic compounds from precursor nanoclusters S_3^0 has been reconstituted as follows: primary chain $S_3^1 \rightarrow$ microlayer $S_3^2 \rightarrow$ microframework S_3^3.

This work is a continuation of studies [1, 16–20] into the modeling of self-organization of systems on the suprapolyhedral level and into the computer-aided geometrical and topological analysis of crystal structures (program package TOPOS).

COMBINATORIAL AND TOPOLOGICAL MODELING OF TETRAHEDRAL PACKINGS

In binary systems A–B, tetrahedral metal clusters can have chemical compositions A_3B, A_2B_2, and AB_3. The highest symmetry of two-color clusters A_3B and AB_3 is described by point group $g = 3m$, and that of cluster A_2B_2 by point group $g = 2mm$. In one chemical system, compositionally different clusters A_3B, A_2B_2, and AB_3 can generate topologically identical crystal structures of intermetallic compounds.

In ternary systems A–B–C, tetrahedral metal clusters can have chemical compositions A_2BC, AB_2C, and ABC_2. In one chemical system, compositionally different clusters A_2BC and AB_2C can generate topologically equivalent crystal structures.

In quaternary systems A–B–C–D, tetrahedral metal clusters have the only possible chemical composition ABCD. Presumably, the number of these chemical systems will be very limited.

Dimeric Clusters $(A_4)_2$

The formation of suprapolyhedral clusters $A_4 + A_4$ is described by the following topological parameters:

Local connectivity index P_{loc}, equal to the number of connections formed between clusters $A_4 + A_4$; and

Total connectivity index P_{tot}, equal to the number of connections formed between primary chains upon microlayer self-assembly and between microlayers upon microframework self-assembly.

Clusters A_4 are involved in primary connection to one another to form dimers $(A_4)_2$. Eleven combinatorially possible variants of connection of one-color clusters $A_4 + A_4$ are shown in Fig. 1. The appearance of two or more connections in dimers that fix the arrangement of tetrahedra $A_4 + A_4$ allows one to classify these interactions with an indication of dimer symmetry.

The number of combinatorially possible variants of involvement of atoms A and B in connecting two-color tetrahedra upon the formation of dimers $AB_3 + AB_3$ and $A_2B_2 + A_2B_2$ increases strongly. Twenty two types of binding of two-color tetrahedra with connectivities $P_{loc} = 4$, 6, and 8 are shown in Fig. 2.

D-1, $P_{loc} = 1$	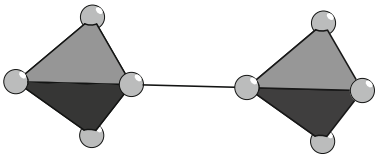	D-7, $P_{loc} = 4$	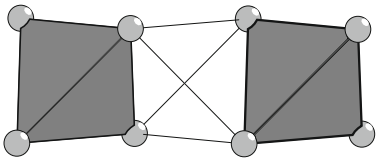
D-2, $P_{loc} = 2$	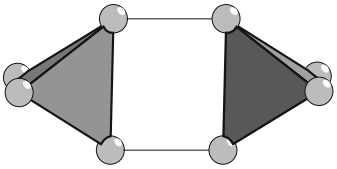	D-8, $P_{loc} = 5$	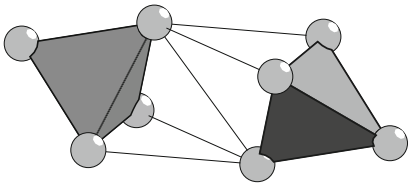
D-3, $P_{loc} = 3$	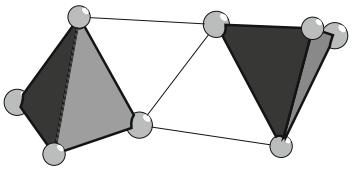	D-9, $P_{loc} = 6$	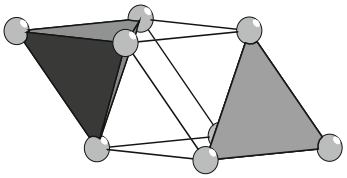
D-4, $P_{loc} = 3$	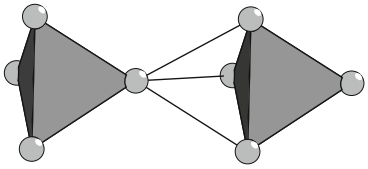	D-10, $P_{loc} = 6$	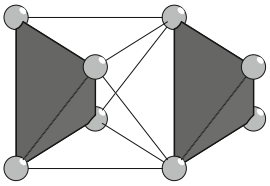
D-5, $P_{loc} = 3$	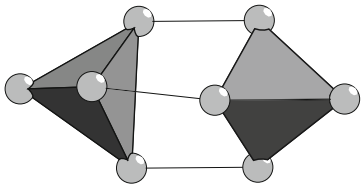	D-11, $4P_{loc} = 8$	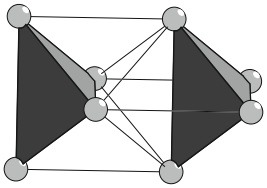
D-6, $P_{loc} = 1$	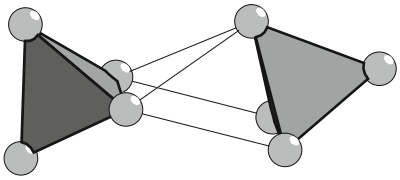		

Fig. 1. Dimers $A_4 + A_4$ with connectivity P_{loc} from 1 to 8.

(a)

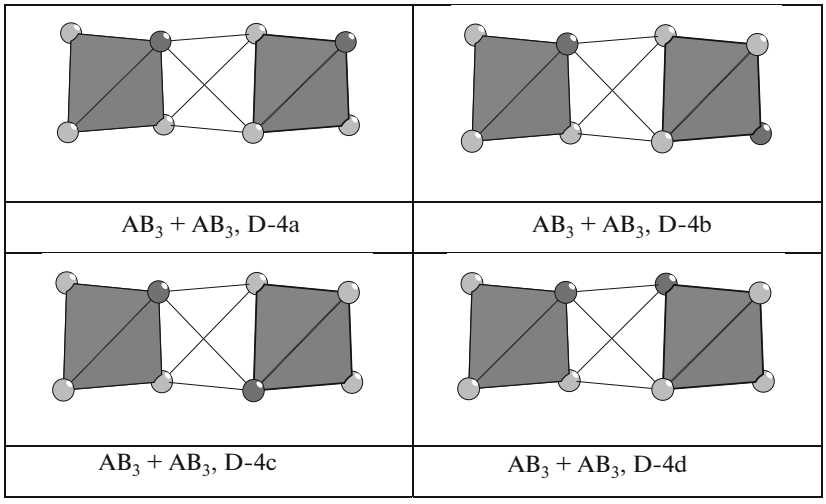

(b)

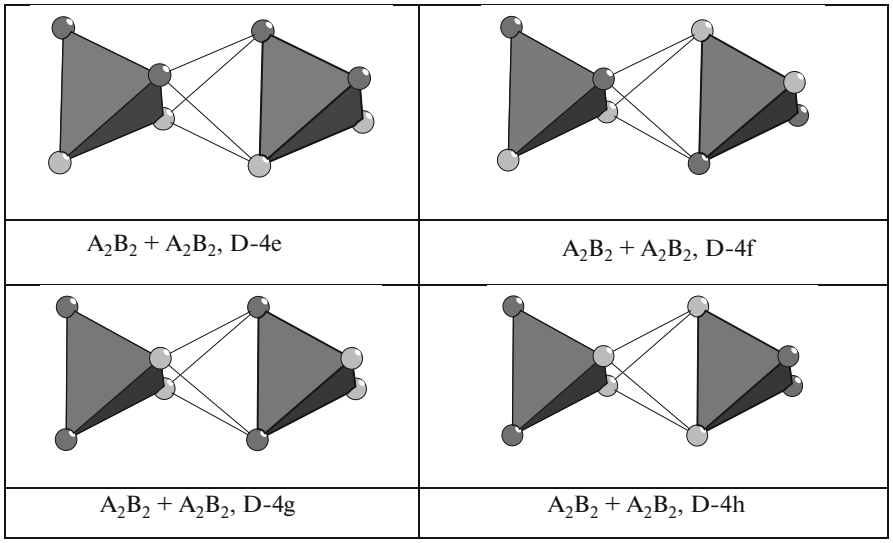

(c)

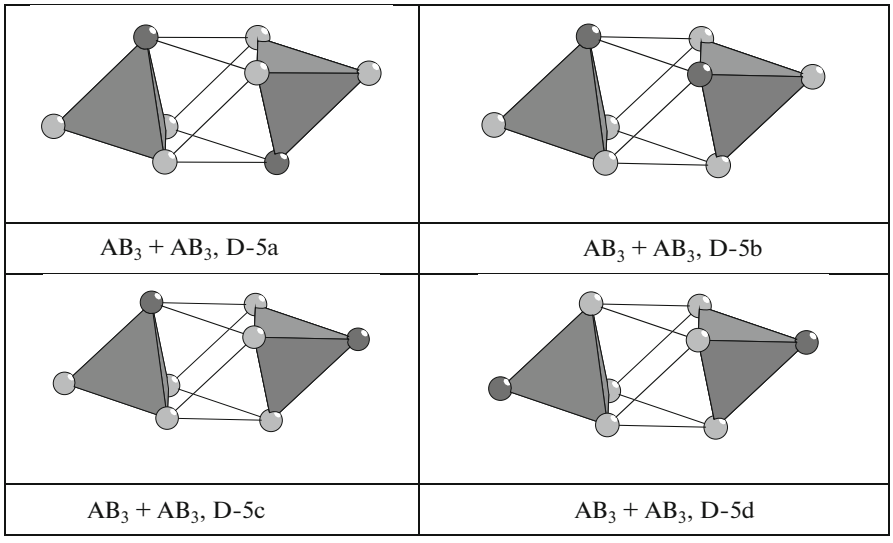

Fig. 2. Dimers $A_3B + A_3B$ and $A_2B_2 + A_2B_2$ with connectivity (a, b) $P_{loc} = 4$, (c, d) $P_{loc} = 6$, and (e, f) $P_{loc} = 8$.

(d)

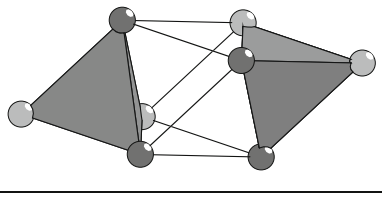

$A_2B_2 + A_2B_2$, D-5e

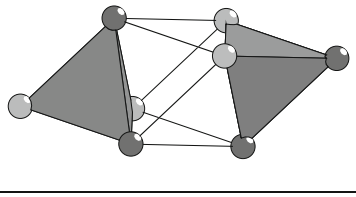

$A_2B_2 + A_2B_2$, D-5f

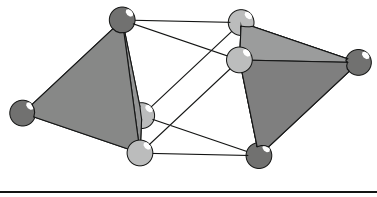

$A_2B_2 + A_2B_2$, D-5g

(e)

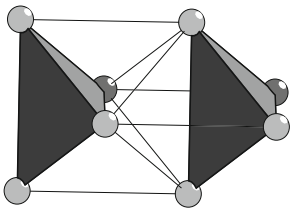

$AB_3 + AB_3$, D-6a

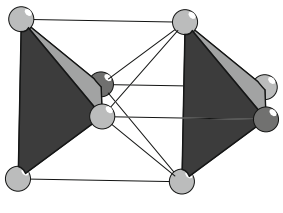

$AB_3 + AB_3$, D-6b

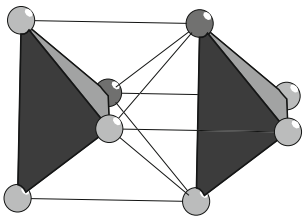

$AB_3 + AB_3$, D-6c

(f)

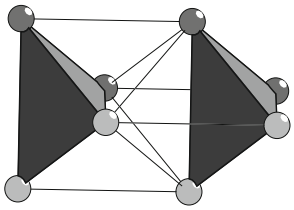

$A_2B_3 + A_2B_2$, D-6d

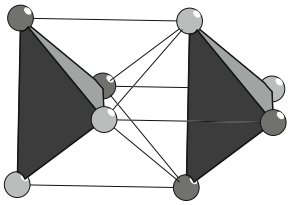

$A_2B_3 + A_2B_2$, D-6e

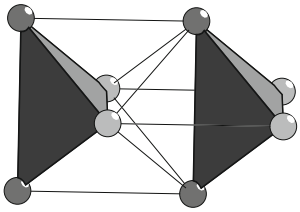

$A_2B_3 + A_2B_2$, D-6f

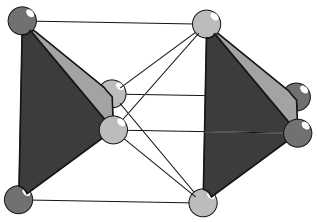

$A_2B_3 + A_2B_2$, D-6g

Fig. 2. (Contd.)

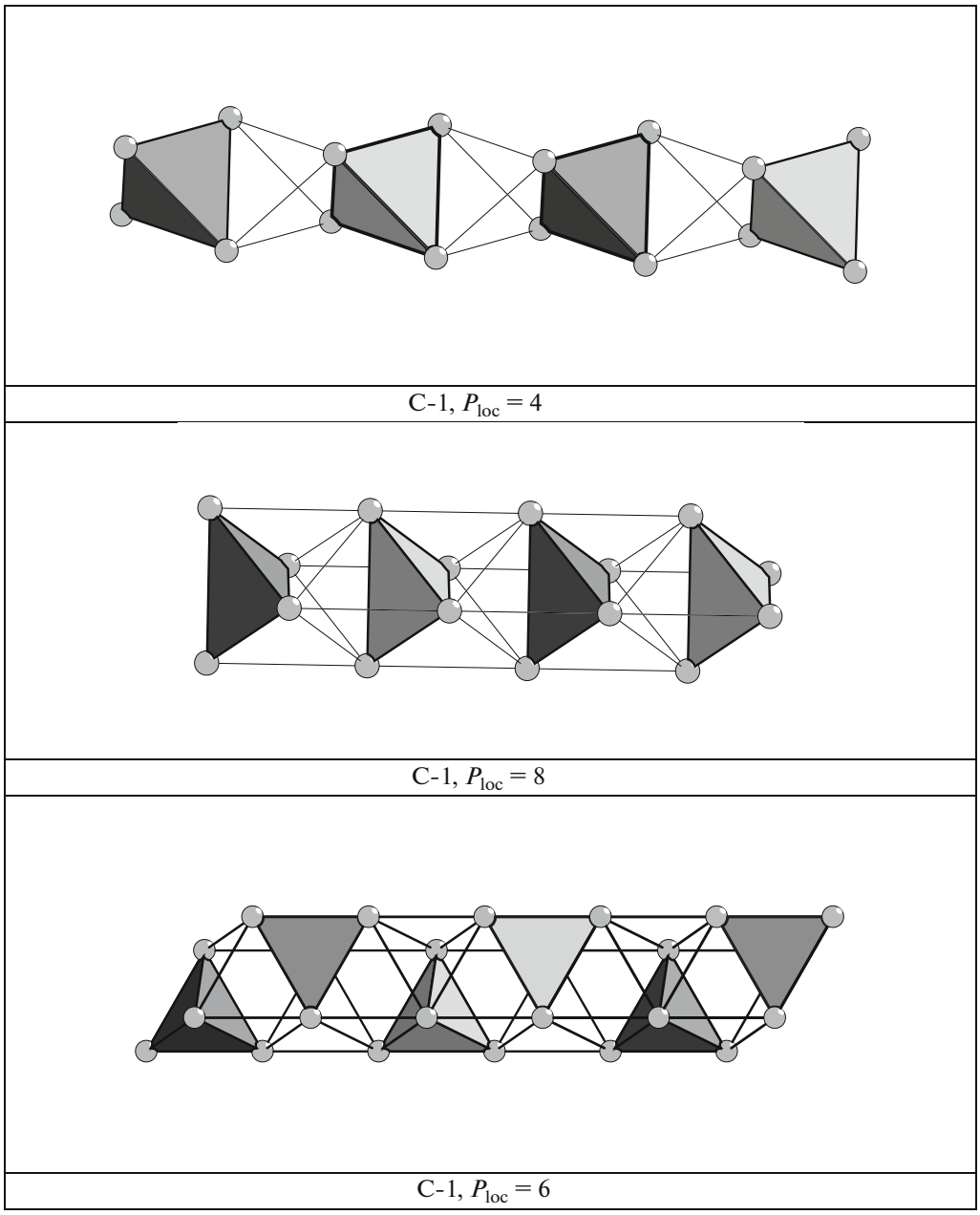

Fig. 3. Primary chains S_3^1.

Self-Assembly of 1D Chains from Dimer Clusters

Let us consider variants of self-assembly of chains built of dimer clusters D-7, D-9, and D-11 with $P_{loc} = 4$, 6, and 8. The identity mechanism is suggested to operate in connections of dimers in the direction of the growth axis of a primary chain with the retention of a constant value of P_{loc} between them.

Two variants of primary chain self-assembly are possible [16–20]:

As a *linear chain* where the centers of all clusters A_4 lie on one straight line, which is the axis of the primary chain, and

As a *zigzag chain*, where the centers of clusters A_4 shift relative to the axis of the primary chain.

Chains built of dimers D-7, D-9, and D-11 with $P_{loc} = 4$, 6, and 8 are shown in Fig. 3. In linear chains C-1 and C-2, all tetrahedra A_4 are connected by translation vectors, which are determined by center-to-center distances between tetrahedra. In *zigzag chain*

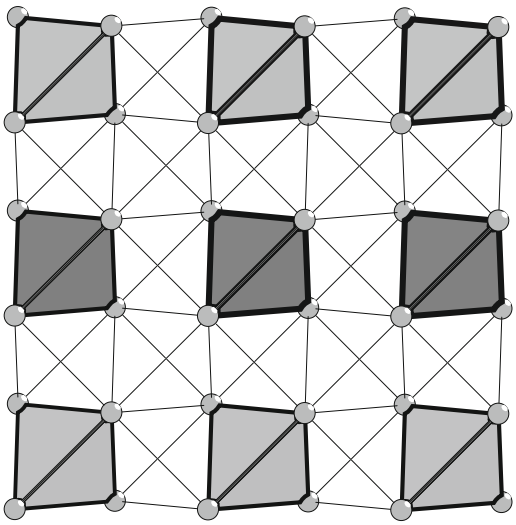

L-1

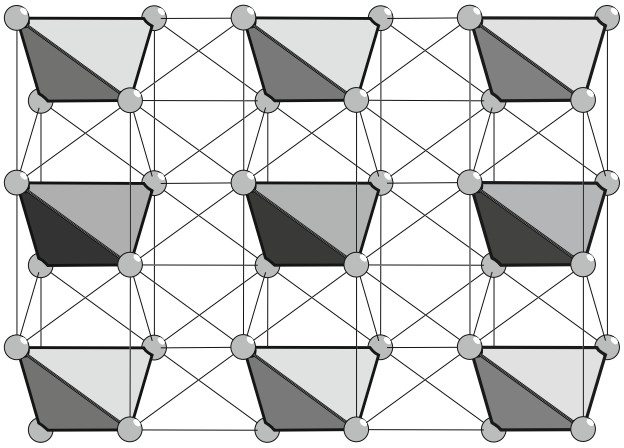

L-2

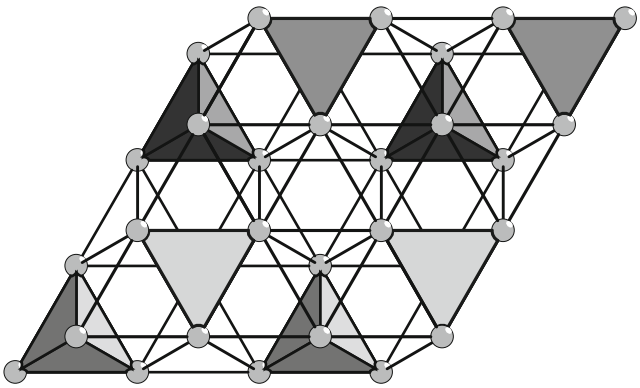

L-3

Fig. 4. Microlayers S_3^2.

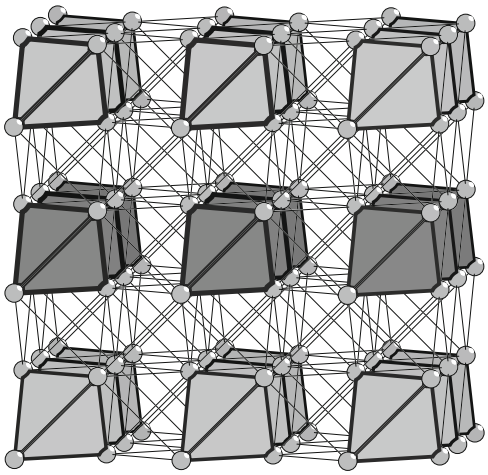

FR-1

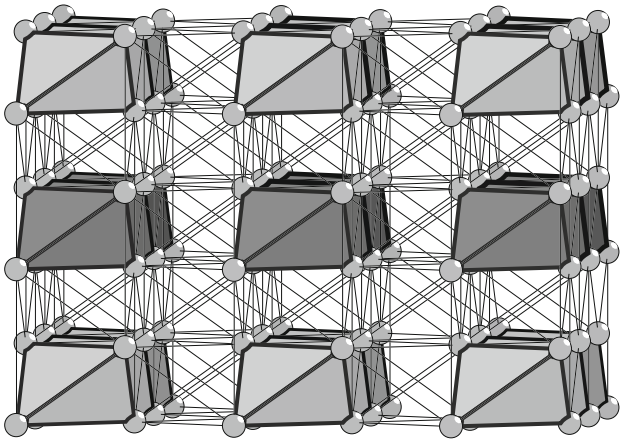

FR-2

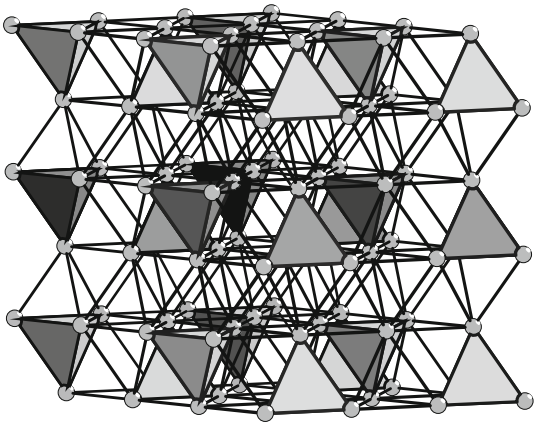

FR-3

Fig. 5. Microframeworks S_3^3.

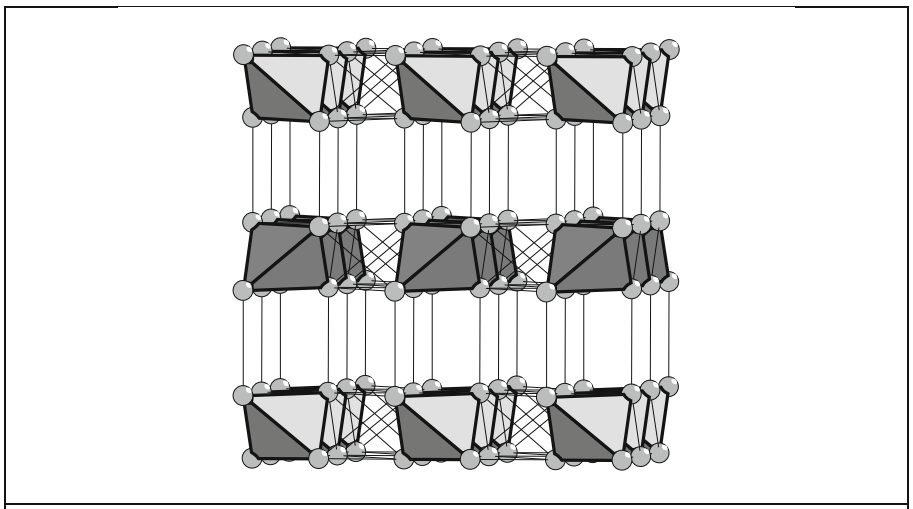

Fig. 5. (Contd.)

C-3, the translation vector connects dimer centers and the translation vector magnitude is determined the distance between them.

Self-Assembly of 2D Microlayers from 1D Chains

The self-assembly scheme of 2D microlayers is as follows:

(1) The position of the main chain is fixed (it is indicated by a darker color in all figures). One replica of the main chain is arranged above the main chain and another is beneath the main chain (both indicated in the figures by a lighter color).

(2) The axes of all chains (the main chain and its replicas) are arranged parallel at equal distances from one another, and the upper chain and lower chain are connected to the central chain so that P_{tot}, the number of connections between the primary chains upon microlayer self-assembly, would be maximal.

Microlayers L-1, L-2, and L-3 built of linear chains C-1, C-2, and C-3 are shown in Fig. 4. The basal 2D network, which characterizes direct connections between the centers of tetrahedra, for layers L-1 and L-2 correspond to network 4.4.4.4., and for layer L-3, to network 6.6.6. (graphite type).

Self-Assembly of 3D Microframeworks from 2D Microlayers

The self-assembly scheme of 3D microframeworks is as follows:

(1) The position of a microlayer is fixed (it is indicated by a darker color in all figures). One replica microlayer is arranged above the microlayer and another beneath the microlayer (both indicated in the figures by a lighter color).

(2) All microlayers (the main microlayer and its replicas) are arranged parallel at equal distances from one another, so the upper microlayer and lower microlayer are connected.

Microframeworks FR-1, FR-2, and FR-3 built of microlayers L-1, L-2, and L-3 are characterized by the greatest number of connections between microlayers (P_{tot}) (Fig. 5). The basal network types, which characterize direct connections between the centers of tetrahedra for frameworks FR-1 and FR-2, correspond to a simple cubic network with CN = 4 + 1 + 1, and for FR-3, to simple hexagonal network with CN = 3 + 1 + 1.

Microframework FR-4, which is built of microlayers L-1, has the number of connections between tetrahedra P_{loc} reduced from 4 to 2 upon their connection by the symmetry plane $g = m$ (Fig. 5). The basal network of microframework FR-4 corresponds to a simple cubic network with CN = 4 + 1 + 1.

COMPUTER-AIDED ANALYSIS PROCEDURES

The geometrical and topological analysis was performed by the program package ToposPro [12, 13], which allows a multi-purpose study of crystal structures in an automatic mode, using their representation in the form of "folded graphs"(factor graphs). Topological types of set local structures FR-1, FR-2, FR-3, and FR-4 was sought among the binary, ternary, and quaternary intermetallic compounds having chemical compositions A_3B, A_2B_2, AB_3, A_2BC, AB_2C, and ABCD, which correspond to a suggested chemical

Table 1. Framework structures FR-1, FR-2, FR-3, and FR-4. The number of representatives and crystallochemical data

Intermetallic compound	Number of representatives	Space group, Pearson's symbol, Wyckoff's sequence	Atom	Local environment	Coordination sequences N_k				
					N_1	N_2	N_3	N_4	N_5
FR-1									
$Cu_{2-x}Au_{2+x}$	397	*Fm*-3*m* (225), *cF*4, *a*	Cu1	Cu and Au	**12**	42	92	162	252
			Au1	Cu and Au	**12**	42	92	162	252
Cu_3Au ($CuAu_3$)	434	*Pm*-3*m* (221), *cP*4, *c a*	Cu1	8Cu + 4Au	12	42	92	162	252
			Au1	12Cu	12	42	92	162	252
Cu_2Au_2	159	*P*4/*mmm* (123), *t*P2, *d a*	Cu1	8Au + 4Cu	**12**	42	92	162	252
			Au1	8 Cu + 4Au	**12**	42	92	162	252
FR-2									
$Cs_{2-x}K_{2+x}$	203	*Im*-3*m* (229), *cI*2, *a*	Cs1	Cs and K	14	50	110	194	302
			K1	Cs and K	14	50	110	194	302
Li_2Hg_2	408	*Pm*-3*m*(221), *cP*2, *b a*	Li1	8Hg + 6Li	14	50	110	194	302
			Hg1	8Li + 6Hg	14	50	110	194	302
Li_3Hg	101	*Fm*-3*m* (225), *cF*16, *c b a*	Li1	8Li + 6Hg	14	50	110	194	302
			Li2	4Hg + 10Li	14	50	110	194	302
			Hg1	14Li	14	50	110	194	302
Na_2Tl_2	7	*Fd*-3*m* (227), *cF*16, *b a*	Na1	4Na + 10Tl	14	50	110	194	302
			Tl1	4Tl + 10Na	14	50	110	194	302
Li_2AgAl	80	*F*-43*m* (216), *cF*16, *d c b a*	Li1	4Li + 6Al + 4Ag	14	50	110	194	302
			Li2	4Li + 4Al + 6Ag	14	50	110	194	302
			Ag1	10Li + 4Ag	14	50	110	194	302
			Al1	10Li + 4Al	14	50	110	194	302
LiMgPdSn	5	*F*-43*m* (216), *cF*16, *d c b a*	Li	4Mg + 6Pd + 4Sn	14	50	110	194	302
			Mg	4Li + 4Pd + 6Sn	14	50	110	194	302
			Pd	6Li + 4Mg + 4Sn	14	50	110	194	302
			Sn	4Li + 6Mg6 + 4Pd	14	50	110	194	302
FR-3									
$Mg_{2-x}Cd_{2+x}$	235	$P6_3/mmc$ (194), *hP*2, *c*	Mg1	Mg and Cd	12	44	96	170	264
			Cd1	Mg and Cd	12	44	96	170	264
$MgCd_3$(Mg_3Cd)	101	$P6_3/mmc$ (194), *hP*8, *h*6 *c*2	Mg1	12Cd	12	44	96	170	264
			Cd1	4Mg + 8Cd	12	44	96	170	264
Cd_2Mg_2	82	*Pmma* (51), o*P*4, *f e*	Mg1	4Mg + 8Cd	12	44	96	170	264
			Cd1	4Cd + 8Mg	12	44	96	170	264
FR-4									
$AuLi_2Sn_2$	3	*I* 41/*amd* (141), *tI*20, *e*2 *b*	Li1	2Li + 7Sn + 2Au	11	39	87	162	237
			Sn1	7Li + 2Sn + 2Au	11	38	88	154	249
			Au1	4Li + 4Sn	8	38	86	152	240

Table 2. Intermetallic compounds with frameworks FR-1, FR-2, FR-3, and FR-4 formed in binary, ternary, and quaternary systems. Structure data for compounds discussed in this work

Intermetallic compound	Space group	Unit cell parameters, A°	V, Å^3	Pearson's symbol	Wyckoff's sequence	CC-ICSD [14]
Binary systems A–B						
Li_3Hg (FR-2)	*Fm*-3*m* (225)	6.561, 6.561, 6.561	282.4	*cF*16	*cba*	104309
Li_2Hg_2 (FR-2)	*Pm*-3*m* (221)	3.294, 3.294, 3.294	35.7	*cP*2	*ba*	104308
$LiHg_3$ (FR-3)	$P6_3/mmc$ (194)	6.240, 6.240, 4.794	161.7	*hP*8	*hc*	639074
Cu_3Au, Auricupride (FR-1)	*Pm*-3*m* (221)	3.753, 3.753, 3.753	52.9	*cP*4	*ca*	40351
Cu_2Au_2,Tetraauri-cupride (FR-1)	*P*4/*mmm* (123)	2.803, 2.803, 3.672	28.9	*tP*2	*da*	611749
$CuAu_3$, Bogdavite (FR-1)	*Pm*-3*m* (221)	4.088, 4.088, 4.088	68.3	*cP*4	*ca*	107220
$CdMg_3$ (FR-3)	$P6_3/mmc$ (194)	6.313, 6.313, 5.074	175.1	*hP*8	*hc*	102025
Cd_2Mg_2 (FR-3)	*Pmma* (51)	5.005, 3.227, 5.277	85.2	*oP*4	*fe*	102022
Cd_3Mg (FR-3)	$P6_3/mmc$ (194)	6.234, 6.234, 5.045	169.8	*hP*8	*hc*	102027
Ternary systems A–B–C						
Li_2AgAl (FR-2)	*F*-43*m* (216)	6.350, 6.350, 6.350	256.0	*cF*16	*dcba*	57330
$LiAg_2Al$ (FR-2)	*F*-43*m* (216)	6.315, 6.315, 6.315	251.9	*cF*16	*dcba*	414342
Li_2RhAl (FR-2)	*F*-43*m* (216)	6.011, 6.011, 6.011	217.2	*cF*16	*dcba*	105509
$LiRhAl_2$ (FR-2)	*F*-43*m* (216)	5.977, 5.977, 5.977	213.5	*cF*16	*dcba*	105508
Li_2PdAl (FR-2)	*F*-43*m* (216)	6.033, 6.033, 6.033	219.6	*cF*16	*dcba*	105505
$LiPdAl_2$ (FR-2)	*F*-43*m* (216)	6.064, 6.064, 6.064	223.0	*cF*16	*dcba*	105504
Li_2AgSn (FR-2)	*F*-43*m* (216)	6.552, 6.552, 6.552	281.3	*cF*16	*dcba*	58318
$LiAg_2Sn$ (FR-2)	*F*-43*m* (216)	6.600, 6.600, 6.600	287.5	*cF*16	*dcba*	154086
Ni_2MnGa (FR-2)	*I* 4/*mmm* (139)	3.865, 3.865, 6.596	98.5	*tI*8	*dba*	153292
Mn_2NiGa (FR-2)	*I* 4/*mmm* (139)	3.915, 3.915, 6.712	102.9	*tI*8	*dba*	187690
Li_2CuSn_2 (FR-4)	$I\,4_1/amd$ (141)	4.428, 4.428, 19.416	380.7	*tI*40	*e2b*	251619
Li_2AuSn_2 (FR-4)	$I\,4_1/amd$ (141)	4.556, 4.556, 19.574	406.3	*tI*40	*e2b*	192982
Li_2AgSn_2 (FR-4)	$I\,4_1/amd$ (141)	4.563, 4.563, 20.182	420.3	*tI*40	*e2b*	426085
Quaternary systems A–B–C–D						
LiMgPdSb (FR-2)	*F*-43*m* (216)	6.341, 6.341, 6.341	255.0	*cF*16	*dcba*	44808
LiMgPtSb (FR-2)	*F*-43*m* (216)	6.308, 6.308, 6.308	251.0	*cF*16	*dcba*	44809
LiMgPtSn (FR-2)	*F*-43*m* (216)	6.397, 6.397, 6.397	261.8	*cF*16	*dcba*	104749
LiMgPdSn (FR-2)	*F*-43*m* (216)	6.420, 6.420, 6.420	264.6	*cF*16	*dcba*	16478
LiMgAuSn (FR-2)	*F*-43*m* (216)	6.465, 6.465, 6.465	270.2	*cF*16	*dcba*	16477

Table 3. Structural types of intermetallic compounds. The number of representatives and crystallochemical data

Intermetallic compound	Number of representatives	Space group, Pearson's symbol, Wyckoff's sequence	Atom	Local environment	Coordination sequences N_k				
					N_1	N_2	N_3	N_4	N_5
Cr_3Si	68	*Pm*-3*n* (223), c*P*8, *ca*	Si1	12Cr	12	50	120	218	344
			Cr1	4 Ge + 10Cr	14	50	114	214	350
Lu_3Co (Fe_3C)	65	*Pnma* (62), c*P*16, dc^2	Co1	9Lu	9	46	104	201	336
			Lu1	3Co + 11Lu	14	53	122	220	352
			Lu2	3 Co + 12Lu	15	54	122	221	344
Ca_2Ge_2 (Cr_2B_2)	145	*Cmcm* (63), (*oC*8, c^2).	Ge1	7Ca + 2Ge	9	44	113	200	333
			Ba1	8Ca + 7Ge	15	54	123	220	339
Y_2Ni_2 (Fe_2B_2)	76	*Pnma* (62), *oP*8, c^2	Ni1	2Ni + 7Y	9	46	110	215	336
			Y1	7Ni + 8Y	15	54	126	221	342
Mg_2Cu_4	241	*Fd*-3*m* (227), *cF*24, *da*	Mg1	12Cu + 4Cu	16	52	130	244	380
			Cu1	6 Cu + 6 Mg	12	50	110	216	356
$MgSnCu_4$	119	*F*-43*m* (216), *cF*24, *eca*	Mg1	4Sn + 12Cu	16	52	130	244	380
			Cu1	3Mg + 6Cu + 3Sn	12	50	110	216	356
			Sn1	4Mg + 12Cu	16	52	130	244	380
Mg_2Zn_4	58	$P6_3/mmc$ (194), *hP*12, *hfa*	Mg1	4Mg + 12Zn	16	52	125	232	358
			Zn1	6Mg + 6Zn	12	50	120	230	374
			Zn2	6Mg + 6Zn	12	50	110	212	348
$(CaCu)Cu_4$	136	*P*6/*mmm* (191), *hP*6, *gca*	Ca1	2Ca + 18Cu	20	62	176	290	488
			Cu1	3Ca + 9Cu	12	50	120	272	428
			Cu2	4Ca + 8Cu	12	56	130	278	434
$AlB_2(ZrBe_2)$	60	*P*6/*mmm* (191), *hP*3, *da*	Al	12B + 6Al	18	62	150	242	414
			B	3B + 6Al	9	53	126	254	366
Ca_2Ge	18	*Pnma* (62), *oP*12, *c*3	Ca1	8Ca + 4 Ge	12	47	113	200	313
			Ca2	10 Ca + 5Ge	15	50	111	202	315
			Ge1	9Ca	9	45	108	192	302
$CaHg_2$	107	*P*6/*mmm* (191) *hP*3, *da*	Ca	2Ca + 12Hg	14	44	104	176	278
			Hg	6Ca + 5Hg	11	47	98	179	275
Co_2Ge (Ni_2In)	111	*P*63/*mmc* (194), *hP*6, *dca*	Co1	8Co + 6Ge	14	44	104	176	278
			Co2	6Co + 5Ge	11	47	98	179	275
			Ge1	11Co	11	47	98	179	275
Cs_2Hg_4	46	I*mma* (74) (*oI12, he*)	Cs1	4Cs + 12Hg	16	50	112	204	322
			Hg1	6Cs + 4Hg	10	50	114	197	309
Ba_4Po_4	67	*Fm*3-*m* (225), *cF*8, *ba*	Ba	12Ba + 6Po	18	18	38	66	102
			Po	6Ba	6	18	38	66	102
Mn_5Ge_3	147	*P*63/*mcm* (193), *hP*16, *g2c*	Mn1	8Mn + 6Ge	14	47	125	224	362
			Mn2	10Mn + 5Ge	15	57	122	229	377
			Ge1	9Mn + 2Ge	11	7	116	229	359
$NaZn_{13}$	55	*Fm*-3*c* (no. 226), *cF*112, *iba*	Na1	24 Zn24	24	62	132	254	384
			Zn1	12 Zn12	12	32	126	188	330
			Zn2	2Na + 10Zn	12	55	129	239	376

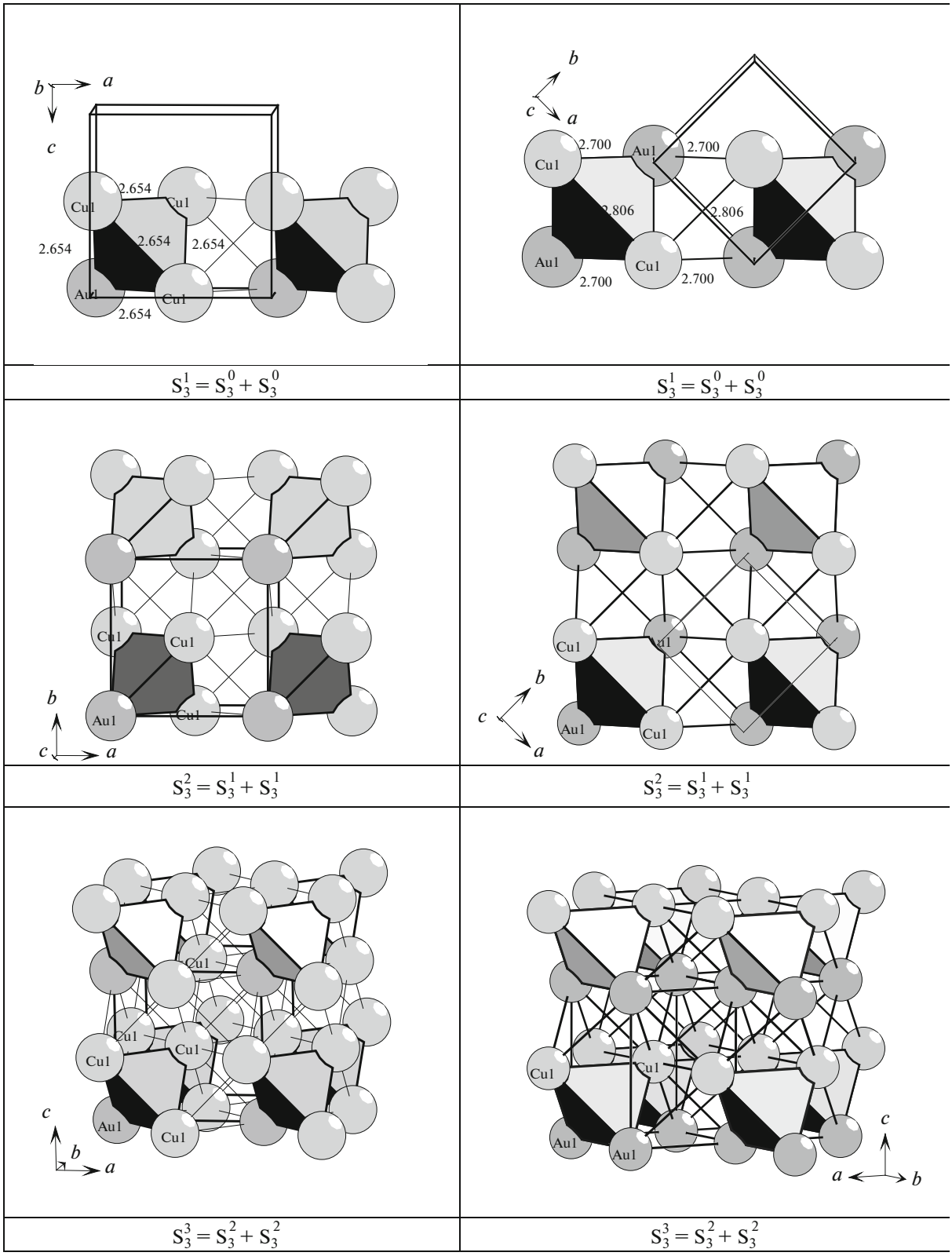

Fig. 6. Crystal structure self-assembly stages for Cu_3Au-*cP*4 (Auricupride), Cu_2Au_2-*tP*2 (Tetraauricupride).

composition of tetrahedral metal precursor clusters (databases ICSD [14] and CRYSTMET [15]).

The geometrical and topological analysis algorithm using the program package ToposPro comprised the following steps:

—calculation of the adjacency matrix in program AutoCN;

—representation of the crystal structure in the form of graph G1, which corresponds to the whole system of atomic bonds, and graph G2, which characterizes the type of basal network of precursor clusters; and

—identification of final subgraphs corresponding to local structures FR-1, FR-2 FR-3, and FR-4 in infinite periodical graphs.

A family of tetrahedral structures of intermetallic compounds comprised of more than 1900 compounds was identified (Tables 1, 2).

In order to identify the precursor nanoclusters in abundant crystal structure types of intermetallic compounds (Table 3), we used special algorithms for partitioning the structural graph into nonintersecting cluster substructures and constructed the basal 3D network of the structure in the form of a graph G2.

The algorithm was implemented in the program package TOPOS [12, 13].

CRYSTAL STRUCTURE SELF-ASSEMBLY FOR INTERMETALLIC COMPOUNDS WITH FRAMEWORKS FR-1, FR-2, FR-3, AND FR-4

Cu_3Au-cP4 (Auricupride) [21] and $CuAu_3$-cP4 (Bogdanovite) [22] Crystal Structures

The type of two-color dimer $AB_3 + AB_3$ (or $A_3B + A_3B$) corresponds to D-7a (with the center in the position 8*g*, symmetry 3*m*). The primary chain corresponds to C-1, the topological type of the resulting layer is L-1, and the topological type of microframework is FR-1 (Fig. 6).

Cu_2Au_2-tP2 (Tetraauricupride) Crystal Structure [23]

The type of two-color dimer $A_2B_2 + A_2B_2$ is D-7e (with the center in the position 4*i*, symmetry *mm2*); the primary chain is C-1; the topological type of the resulting layer is L-1, and the topological type of microframework is FR-1 (Fig. 6).

$(Cu,Au)_4$-cF4 Crystal Structure

The topological type of microframework corresponds to FR-1 and is characterized by various variants of local interactions upon connection of tetrahedra $Cu_{2-x}Au_{2+x}$. It is only for the melts whose chemical composition is Cu_3Au, Cu_2Au_2, or Cu_3Au that slow cooling gives generates crystal structures with the specified type of local interactions of tetrahedral metal clusters.

$CdMg_3$-hP8 [24] and Cd_3Mg-hP8 [24] Crystal Structures

The type of two-color dimer $AB_3 + AB_3$ is D-9a (with the center in the position 6*g*, symmetry 2/*m*); the primary chain is C-3, the topological type of the resulting layer is L-3, and the topological type of microframework is FR-3 (Fig. 7).

Cd_2Mg_2-oP4 Crystal Structure [25]

The type of two-color dimer $A_2B_2 + A_2B_2$ is D-9e (with the center in the position 2*b*, symmetry 2/*m*); the primary chain is C-3; the topological type of the resulting layer is L-3, and the topological type of microframework is FR-3 (Fig. 7).

FR-3: $(Mg,Cd)_4$-hP2 Crystal Structure [26]

The topological type of microframework is FR-3 with various variants of local interactions upon connection of tetrahedra $Mg_{2-x}Cd_{2+x}$. It is only for the melts whose chemical composition is Mg_3Cd, Mg_2Cd_2, or $MgCd_3$ that crystal structures are formed with the specified type of local interactions between tetrahedral metal clusters.

Li_3Hg-cF16 Crystal Structure [27]

The type of two-color dimer $AB_3 + AB_3$ is D-11a (with the center in the position 96*j*, symmetry *m*); the primary chain is C-2; the topological type of the resulting layer is L-2, and the topological type of microframework is FR-2 (Fig. 8).

Li_2Hg_2-cP2 Crystal Structure [28]

The type of two-color dimer $A_2B_2 + A_2B_2$ is D-11d (with the center in the position 12*h*, symmetry is *mm*2); the primary chain is C-2; the topological type of the resulting layer is L-2, and the topological type of microframework is FR-2 (Fig. 8).

Cu_3Zn-cF4, a Crystal Structure [29]

The topological type of microframework corresponds to FR-2, characterized by various variants of local interactions upon connection of tetrahedra Cu_3Zn.

Na_2Tl_2-cF16 Crystal Structure [30]

This crystallochemical family comprises seven compounds: Li_2M_2 (where M = Al, Ga, In, Zn, Cd) and Na_2M_2 (where M = In, Tl).

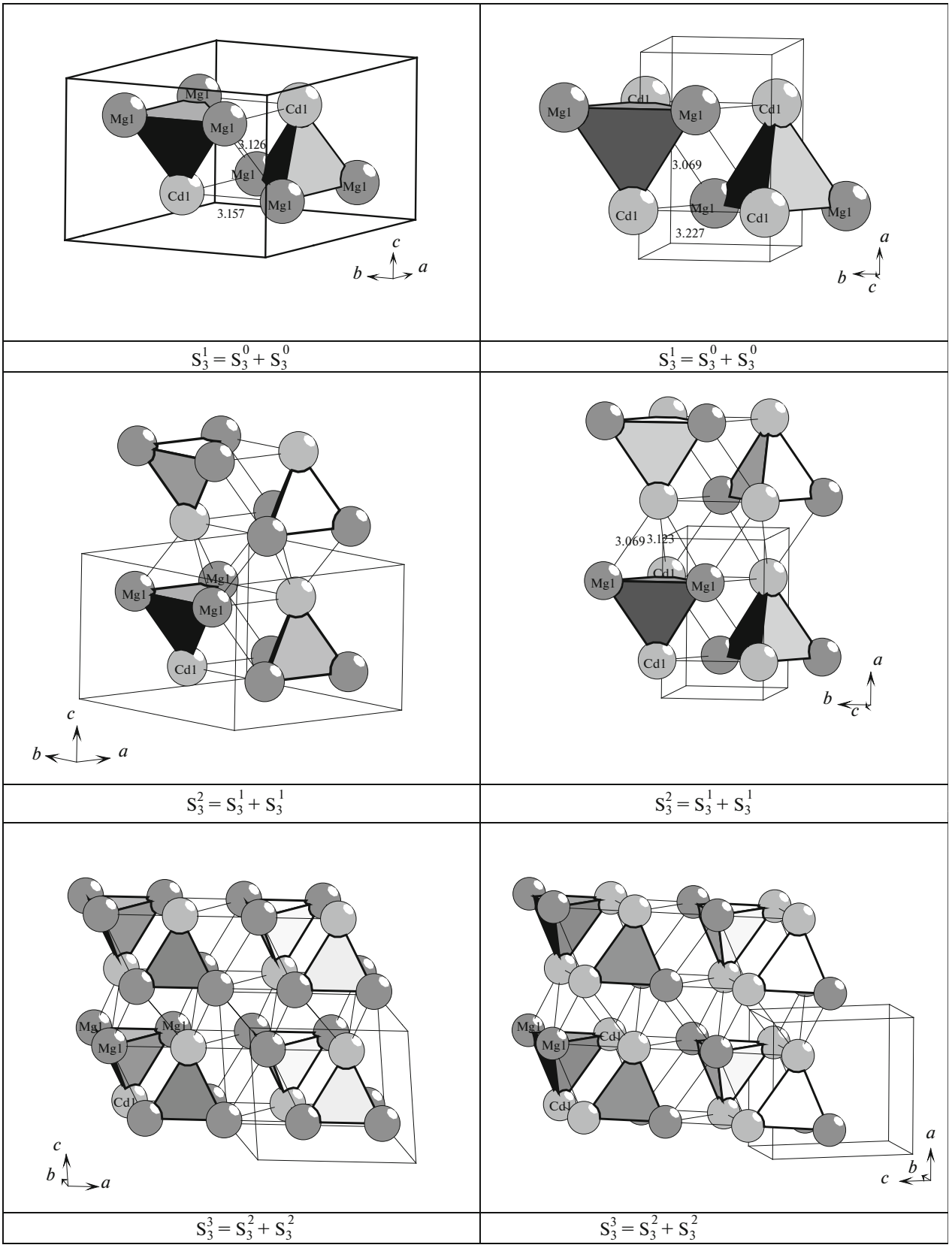

$S_3^1 = S_3^0 + S_3^0$ | $S_3^1 = S_3^0 + S_3^0$

$S_3^2 = S_3^1 + S_3^1$ | $S_3^2 = S_3^1 + S_3^1$

$S_3^3 = S_3^2 + S_3^2$ | $S_3^3 = S_3^2 + S_3^2$

Fig. 7. Crystal structure self-assembly stages for $CdMg_3$-*hP*8 with hexagonal symmetry and Cd_2Mg_2-*oP*4 with orthorhombic symmetry.

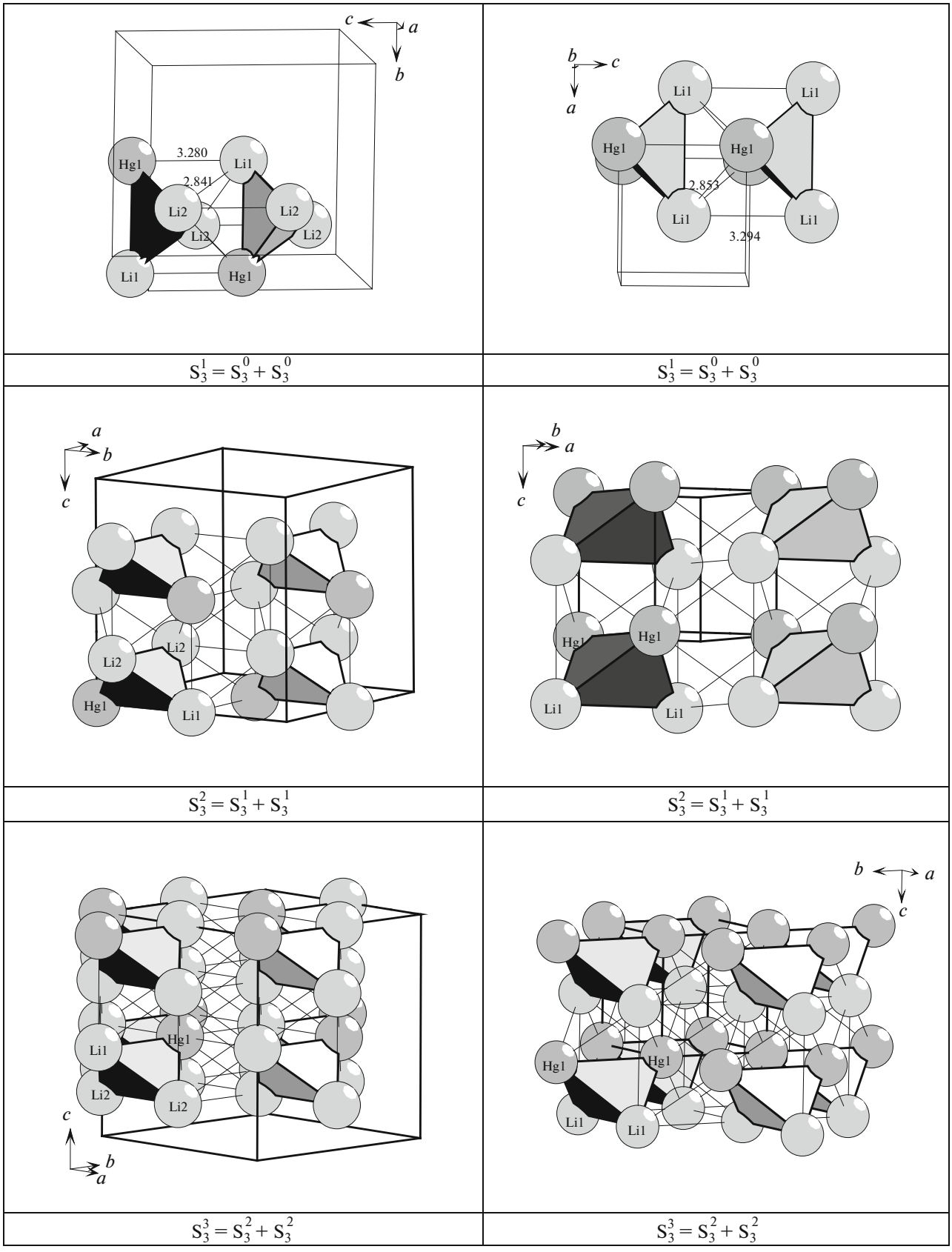

$S_3^1 = S_3^0 + S_3^0$ | $S_3^1 = S_3^0 + S_3^0$

$S_3^2 = S_3^1 + S_3^1$ | $S_3^2 = S_3^1 + S_3^1$

$S_3^3 = S_3^2 + S_3^2$ | $S_3^3 = S_3^2 + S_3^2$

Fig. 8. Crystal structure self-assembly stages for Li_3Hg-*cF*16 and Li_2Hg_2-*cP*2.

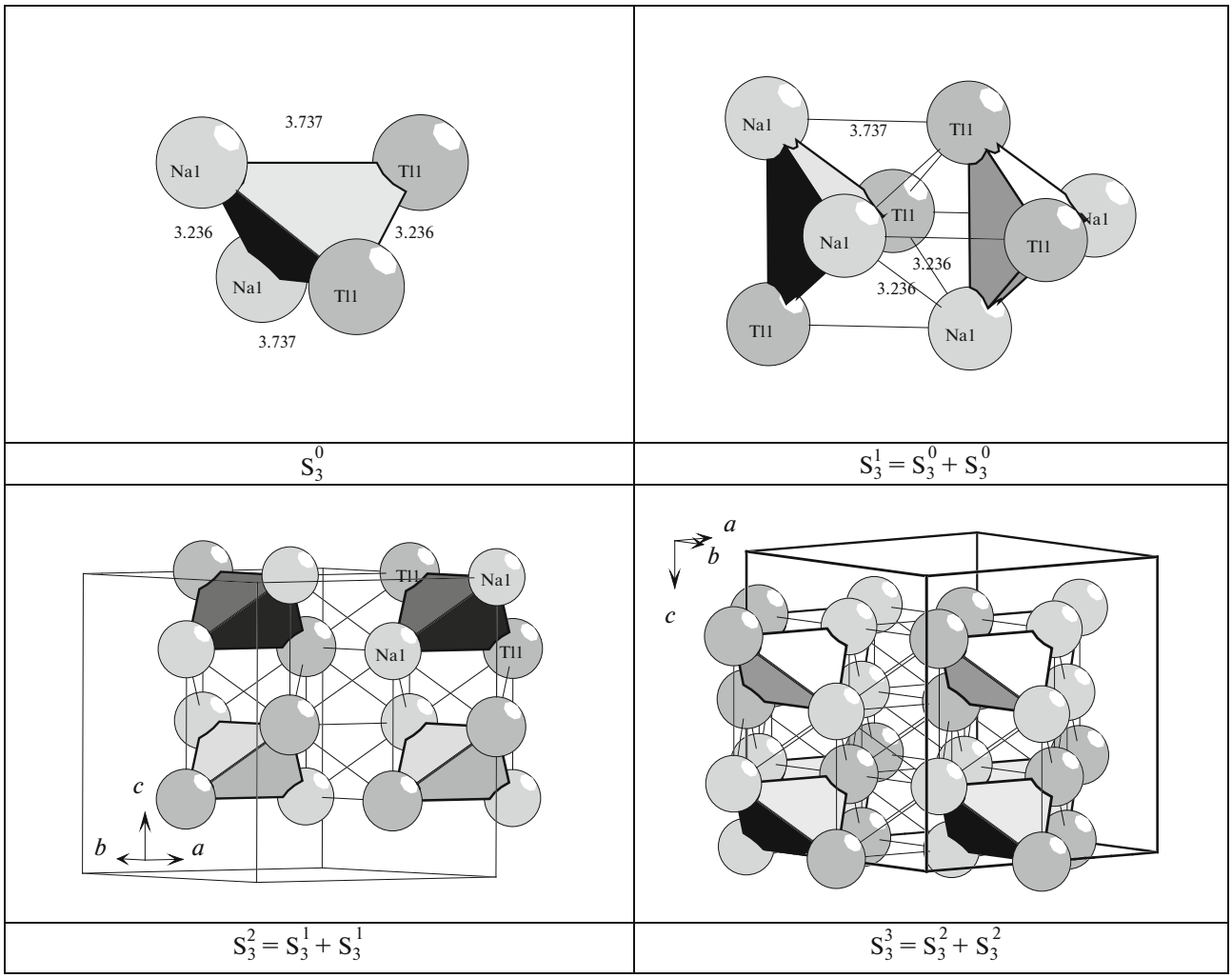

Fig. 9. Crystal structure self-assembly stages for Na_2Tl_2-*cF*16.

The type of two-color dimer $A_2B_2 + A_2B_2$ is D-6e (with the center in the position 96*h*, symmetry 2) (Fig. 9). the primary chain is C-2, the topological type of layer is L-2, and the topological type of microframework is FR-2 (Fig. 10).

Li_2AgAl-cF16 [31] and $LiAg_2Al$-cF16 [32] Crystal Structures

Framework structures FR-2 were identified in the system Li-Ag–Al for intermetallic compounds having chemical compositions of Li_2AgAl and $LiAg_2Al$ (Fig. 10).

LiMgPdSn-cF16 Crystal Structure [33]

Framework structures FR-2 of the type LiMgPdSn were identified for five intermetallic compounds in quaternary systems (Fig. 10, Table 2).

Li_2Sn_2Au-tI40 Crystal Structure

This crystallochemical family comprises three representatives: Li_2AuSn_2-*tI*40 [34], Li_2CuSn_2-*tI*40 [35], and Li_2AgSn_2-*tI*40 [35].

The type of two-color dimer $A_2B_2 + A_2B_2$ is D-4e (with the center in the position 16f, symmetry 2), the primary chain is C-1; the topological type of the resulting layer is L-1, and the topological type of microframework is FR-4 (Fig. 11).

SELF-ASSEMBLY OF MOST ABUNDANT CRYSTAL STRUCTURE TYPES OF INTERMETALLIC COMPOUNDS

Crystallochemical data and the number of representatives of the types of intermetallic compounds under consideration are found in Table 3.

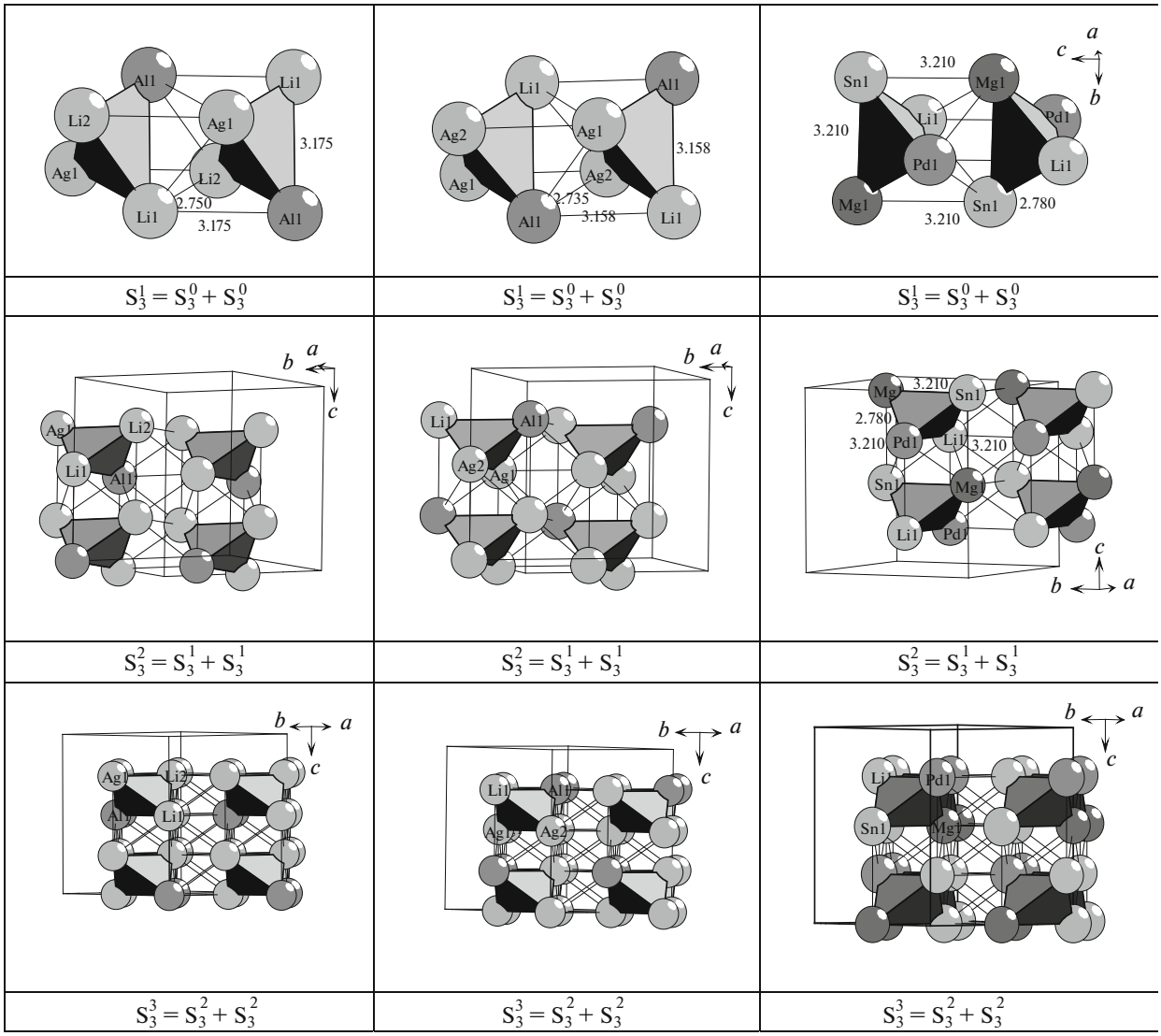

Fig. 10. Crystal structure self-assembly stages for Li_2AgAl-*cF*16, $LiAg_2Al$-*cF*16, and LiMgPdSn-*cF*16.

Cr_3Si Crystal Structure [36]

The cubic unit cell parameters: $a = 4.560$ Å, $V = 94.81$ Å^3, $Z = 2$, space group *Pm*-3*n* (no. 223). Point symmetry elements: *m*-3, *mmm*, -4*m*2, etc.

In a unit cell, there are two precursor clusters Cr_3Si (Fig. 12). The center of a tetrahedral precursor cluster Cr_3Si is in the special position 24*k* (0.31, 0, 1/8) with point symmetry $g = 2$. The center of a suprapolyhedral precursor cluster $(Cr_3Si)_2$ is in the general position 48*l* (0.56, 0.19, 0.31). The connectivity index of tetrahedra Cr_3Si in the suprapolyhedral cluster is seven, nine in the direction of axis *x*, and seven in the direction of axis *z* (Fig. 12).

The basal 3D network corresponding to the centers of mass of the suprapolyhedral precursor cluster $(Cr_3Si)_2$ corresponds to a cubic network with CN = 6 and a basal 2D network of type 4^4 (Fig. 12).

Primary chain. Primary chains are self-assembled of clusters $(Cr_3Si)_2$ in the direction of axis *xy* (Fig. 12) with the connectivity index $P_{loc} = 9$. The center-to-center distance between suprapolyhedral clusters corresponds to the translation vector magnitude **a** = 4.560 Å.

Microlayer self-assembly. Microlayer S_3^2 is formed via connection of two parallel lying primary chains in plane *xy* (Fig. 12). The center-to-center distance between suprapolyhedral clusters $(Cr_3Si)_2$ corresponds to the translation vector magnitude **b** = 4.560 Å.

Microframework self-assembly. Microframework S_3^3 is formed via connection of two microlayers (Fig. 12). The distance between microlayers determines the translation vector magnitude **c** = 4.560 Å.

Lu_3Co Crystal Structure [37]

The orthorhombic unit cell parameters: $a = 6.870$ Å, $b = 9.030$ Å, $c = 6.140$ Å, $V = 380.9$ Å^3, $Z = 4$, space group *Pnma* (no. 62), group order 8. Point symmetry elements: $g = -1$ and m. In a unit cell, there are four tetrahedral precursor clusters Lu_3Co (Fig. 13). The center of a precursor cluster Lu_3Co is in the special position 4*c* (0.20, ¼, 0.357) with symmetry $g = m$.

The basal 3D cubic network with CN = 6 and basal 2D network 4^4.

Primary chain. Self-assembly of primary chains from tetrahedral clusters Lu_3Co occurs in the direction of axis *x* (Fig. 13) with the connectivity index $P_{loc} = 6$. The center-to-center distance between tetrahedral clusters T_4 determines the translation vector magnitude **a/2** = 6.870/2 Å.

Microlayer self-assembly. Microlayer S_3^2 is formed via connection of primary chains in plane (011), $g = -1$, the position 4*a* (½, ½, ½). The connectivity index $P_{loc} = 7$. The center-to-center distance between tetrahedral clusters Lu_3Co from neighboring chains determines the translation vector magnitude **b**/2 = 9.030/2 Å (Fig. 13).

Microframework self-assembly. Microframework S_3^3 is formed via connection of two microlayers $g = -1$ (4*b*, ½, ½, 0) (Fig. 13). The distance between microlayers determines the translation vector magnitude **c** = 6.140 Å.

Cr_2B_2 [38] Crystal Structure

The orthorhombic unit cell parameters: $a = 2.978$ Å, $b = 7.879$ Å, $c = 2.934$ Å, $V = 68.86$ Å^3, $Z = 2$, space group *Cmcm* (no. 63), group order 16. Point symmetry elements: $2/m$, $m2m$, -1, etc.

In a unit cell, there are two tetrahedral precursor clusters Cr_2B_2 (Fig. 14). The center of a precursor cluster Cr_2B_2 is in the special position 8*e* (3/4, 0, 0) with point symmetry $g = 2$.

The basal 3D cubic network with CN= 6 and basal 2D network 4^4 (Fig. 14).

Primary chain. Self-assembly of primary chains from tetrahedral clusters Cr_2B_2 occurs in the direction of axis *z* (Fig. 14) with the connectivity index $P_{loc} = 4 + 2$. The center-to-center distance between clusters Cr_2B_2 corresponds to the shortest translation vector **c** = 2.934 Å.

Microlayer self-assembly. Microlayer S_3^2 is formed via connection of two parallel lying primary chains in plane *xz* (Fig. 14). The center-to-center distance between clusters Cr_2B_2 from neighboring chains corresponds to the translation vector magnitude **a** = 2.978 Å.

Microframework self-assembly. Microframework S_3^3 is formed via connection of two microlayers (Fig. 3). The

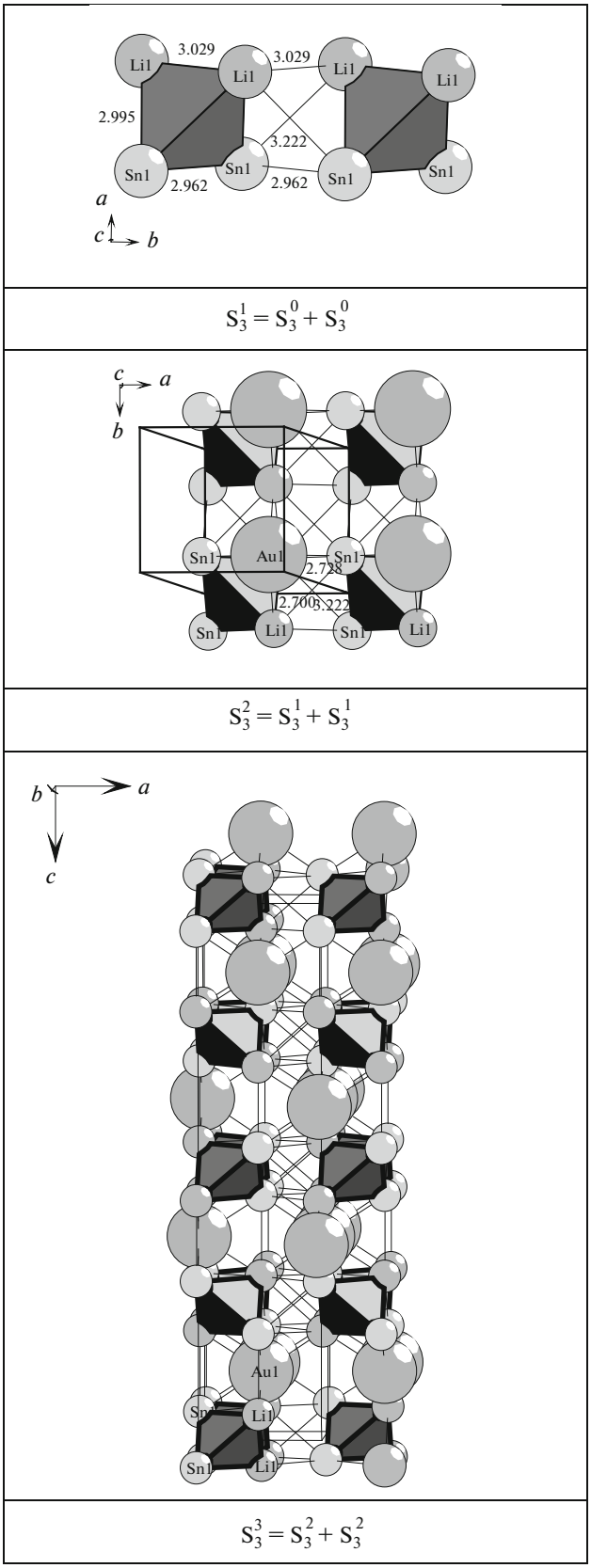

Fig. 11. Li_2Sn_2Au-*cF*16. Crystal structure self-assembly stages.

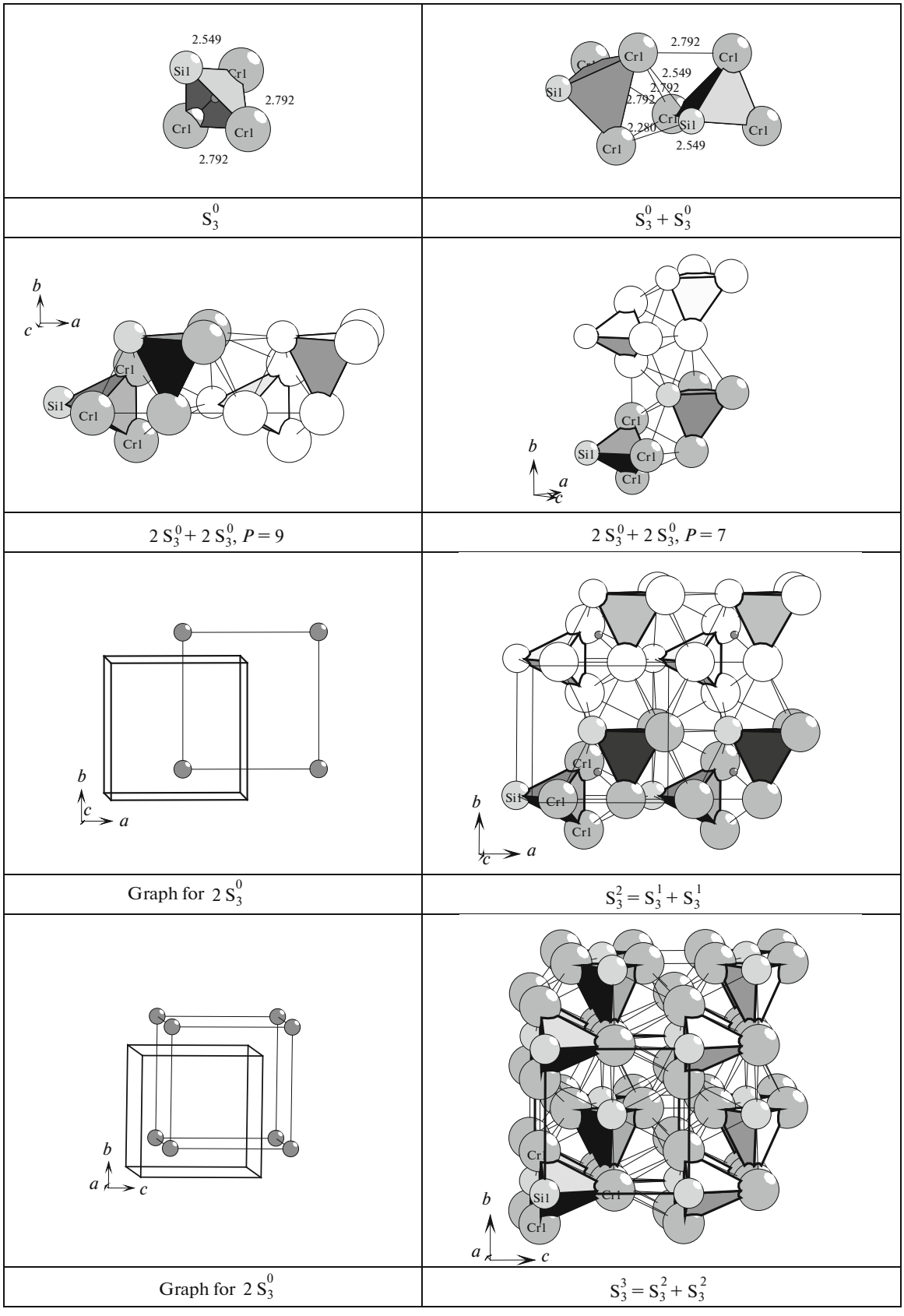

Fig. 12. Cr_3Si. Crystal structure self-assembly stages.

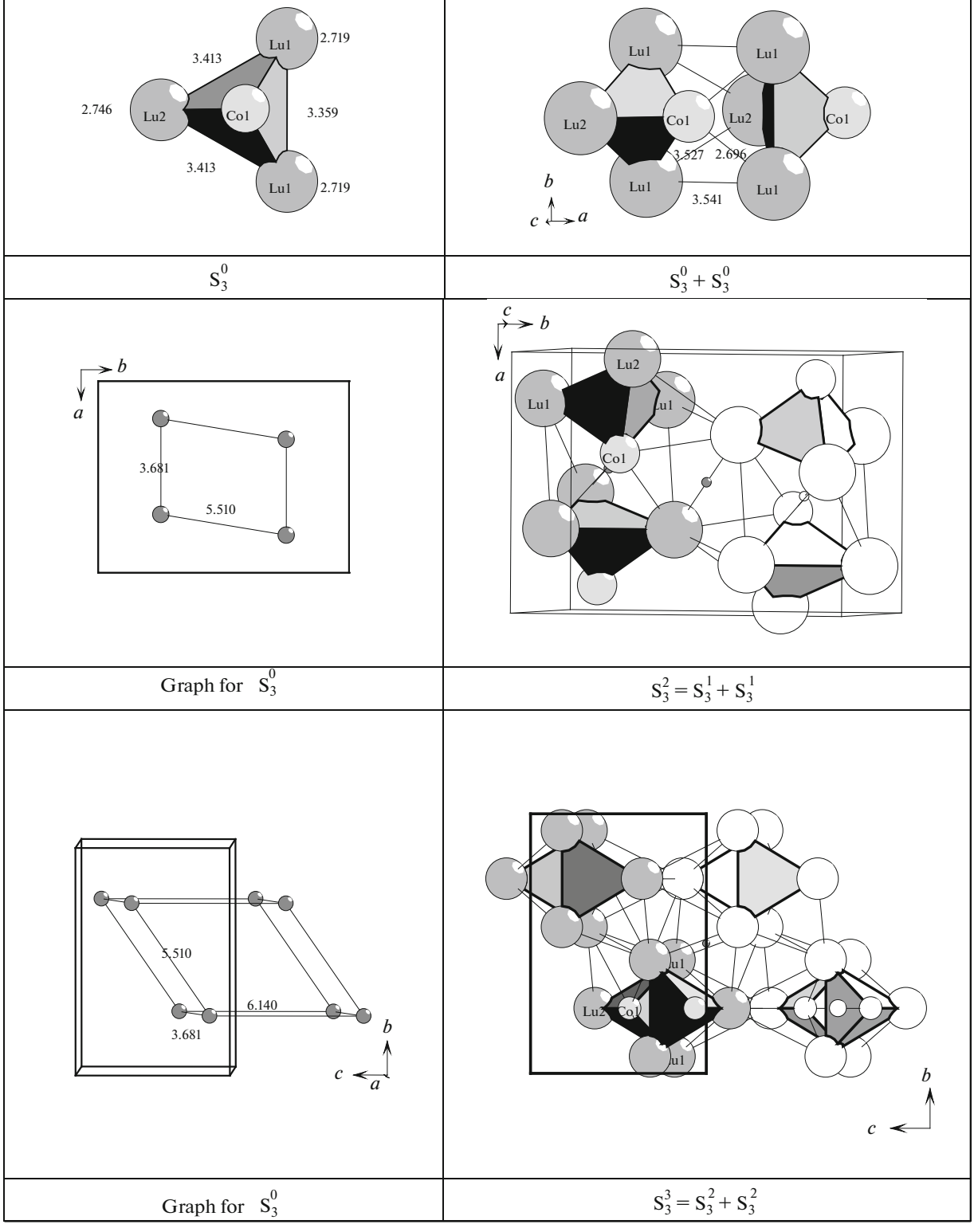

Fig. 13. Lu_3Co. Crystal structure self-assembly stages.

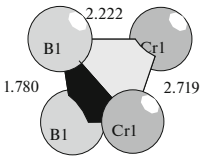

S_3^0

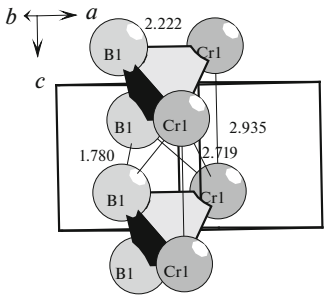

S_3^1

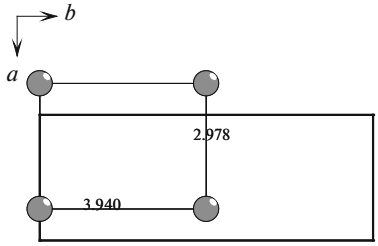

Graph for S_3^0

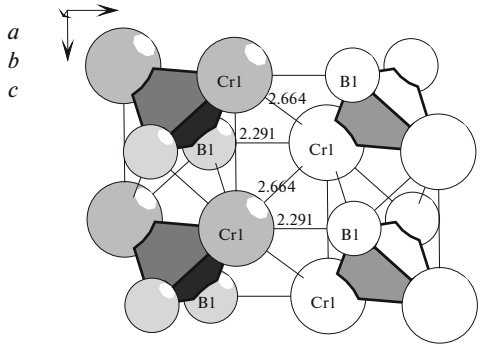

$S_3^2 = S_3^1 + S_3^1$, $P = 7$

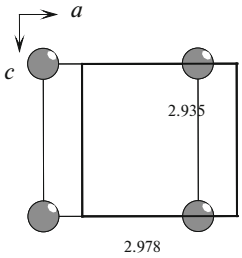

Graph for S_3^0

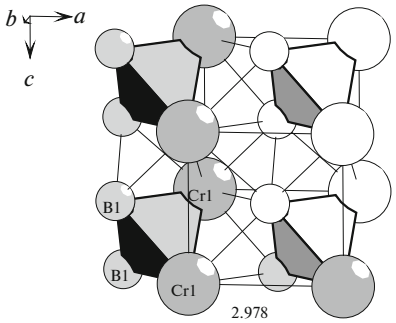

$S_3^2 = S_3^1 + S_3^1$, $P = 12$

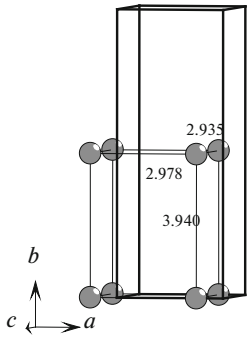

Graph for S_3^0

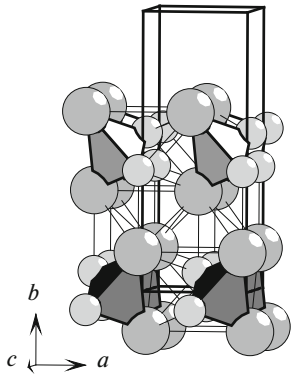

$S_3^3 = S_3^2 + S_3^2$

Fig. 14. Cr_2B_2. Crystal structure self-assembly stages. Figures denote distances in angstroms.

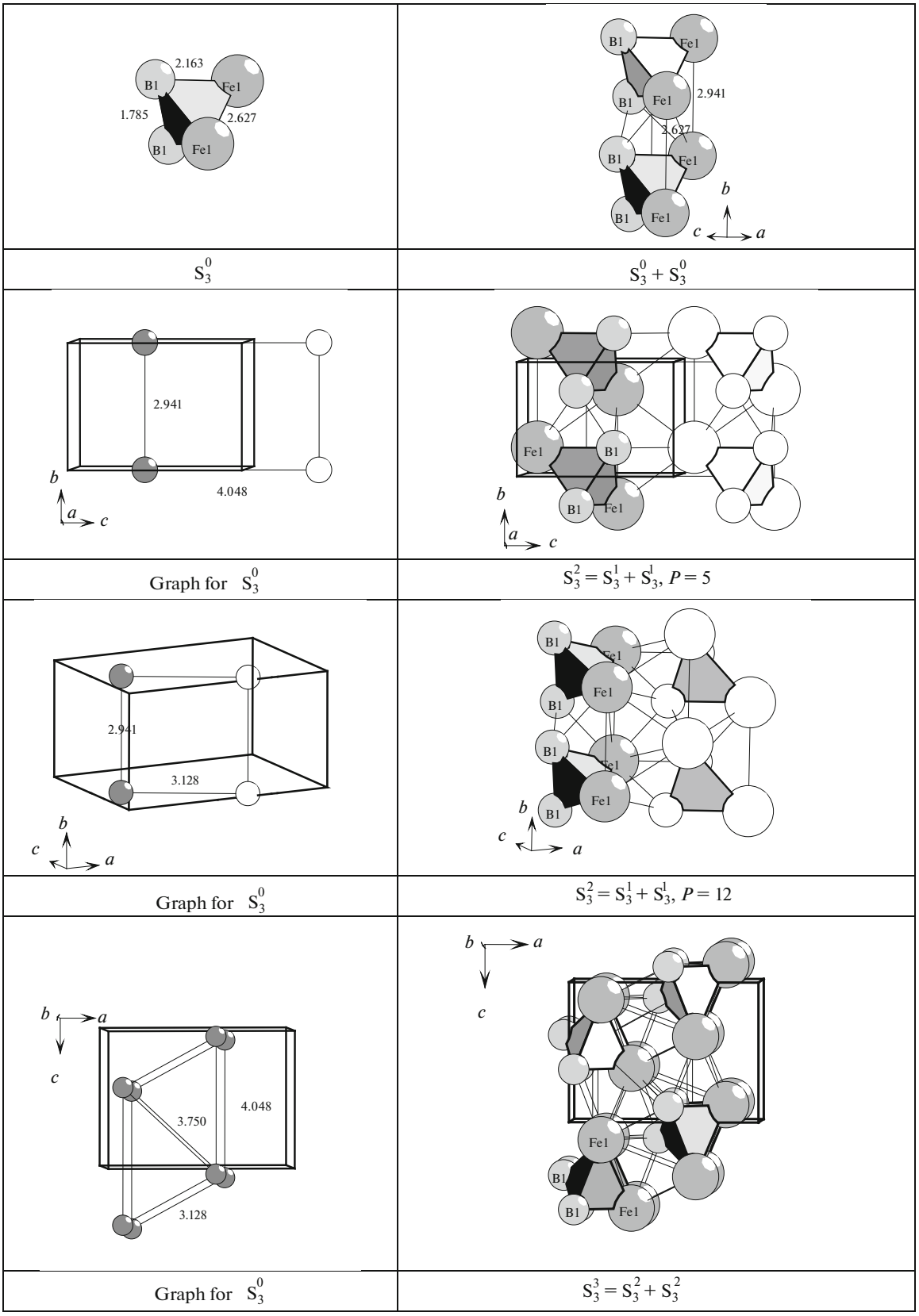

S_3^0	$S_3^0 + S_3^0$
Graph for S_3^0	$S_3^2 = S_3^1 + S_3^1$, $P = 5$
Graph for S_3^0	$S_3^2 = S_3^1 + S_3^1$, $P = 12$
Graph for S_3^0	$S_3^3 = S_3^2 + S_3^2$

Fig. 15. Fe_2B_2. Crystal structure self-assembly stages. Figures denote distances in angstroms.

(a)

Li											Be			
Na											Mg	Al		
K	Ca	Sc	Ti	V	Cr	Mn	Fe	Co	Ni	Cu	Zn	Ga	Ge	
Rb	Sr	Y	Zr	Nb	Mo	Tc	Ru	Rh	Pd	Ag	Cd	In	Sn	Sb
Cs	Ba	La	Hf	Ta	W	Re	Os	Ir	Pt	Au	Hg	Tl	Pb	Bi
Fr	Ra													

(b)

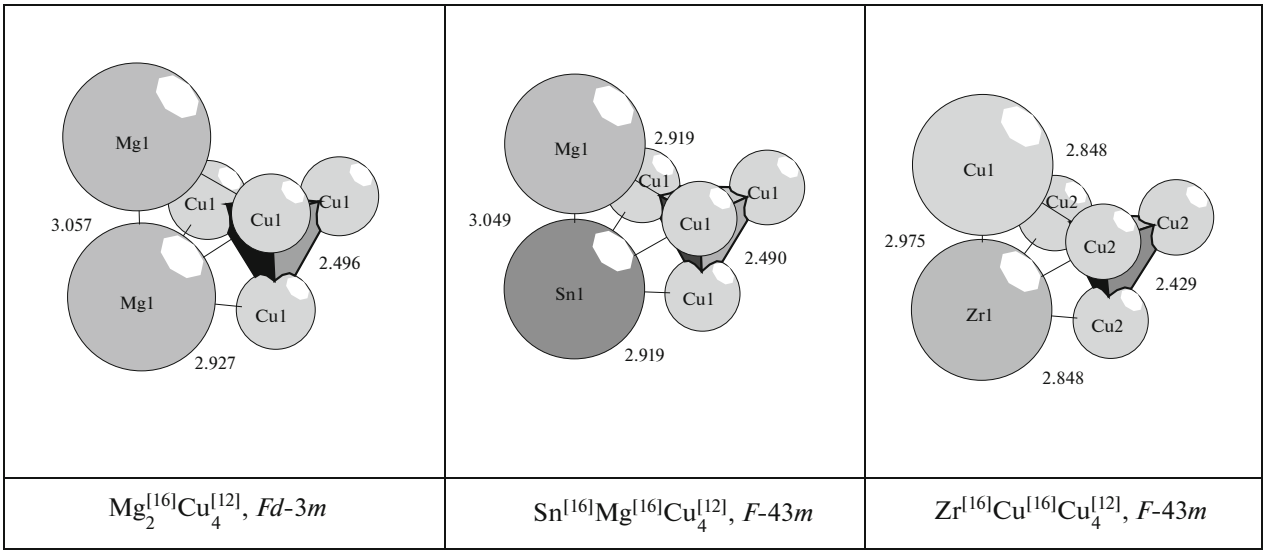

$Mg_2^{[16]}Cu_4^{[12]}$, *Fd*-3*m*	$Sn^{[16]}Mg^{[16]}Cu_4^{[12]}$, *F*-43*m*	$Zr^{[16]}Cu^{[16]}Cu_4^{[12]}$, *F*-43*m*

Fig. 16. (a) The Periodic Table with indicated atoms that form tetrahedral metal clusters B_4. Template atoms are in the beginning of each row. The bifunctional crystallization behavior is intrinsic to such atoms as Be, Ni, Cu, Pt, Ir, and Au, which enter tetrahedra B_4 and are template atoms A. (b) Precursor clusters. Figures denote distances in angstroms. (c) Crystal structure self-assembly stages for $MgSnCu_4$.

distance between microlayers corresponds to the translation vector magnitude **b/2** = 7.879/2 Å.

Fe_2B_2 Crystal Structure [39]

The orthorhombic unit cell parameters: $a = 5.495$ Å, $b = 2.941$ Å, $c = 4.048$ Å, $V = 65.41$ Å^3, $Z = 2$, space group *Pnma* (no. 62), group order 8. Point symmetry elements: -1 and m.

In a unit cell, there are two tetrahedral precursor clusters Fe_2B_2 (Fig. 15). The center of a precursor cluster is in the general position 8*d* (0.625, 0, 0.065).

The basal 3D cubic network with CN = 6 and basal 2D network 4^4 (Fig. 15).

Primary chain. Self-assembly of primary chains from tetrahedral clusters Fe_2B_2 occurs in the direction of axis z (Fig. 15) with the connectivity index P_{loc} =

(b)

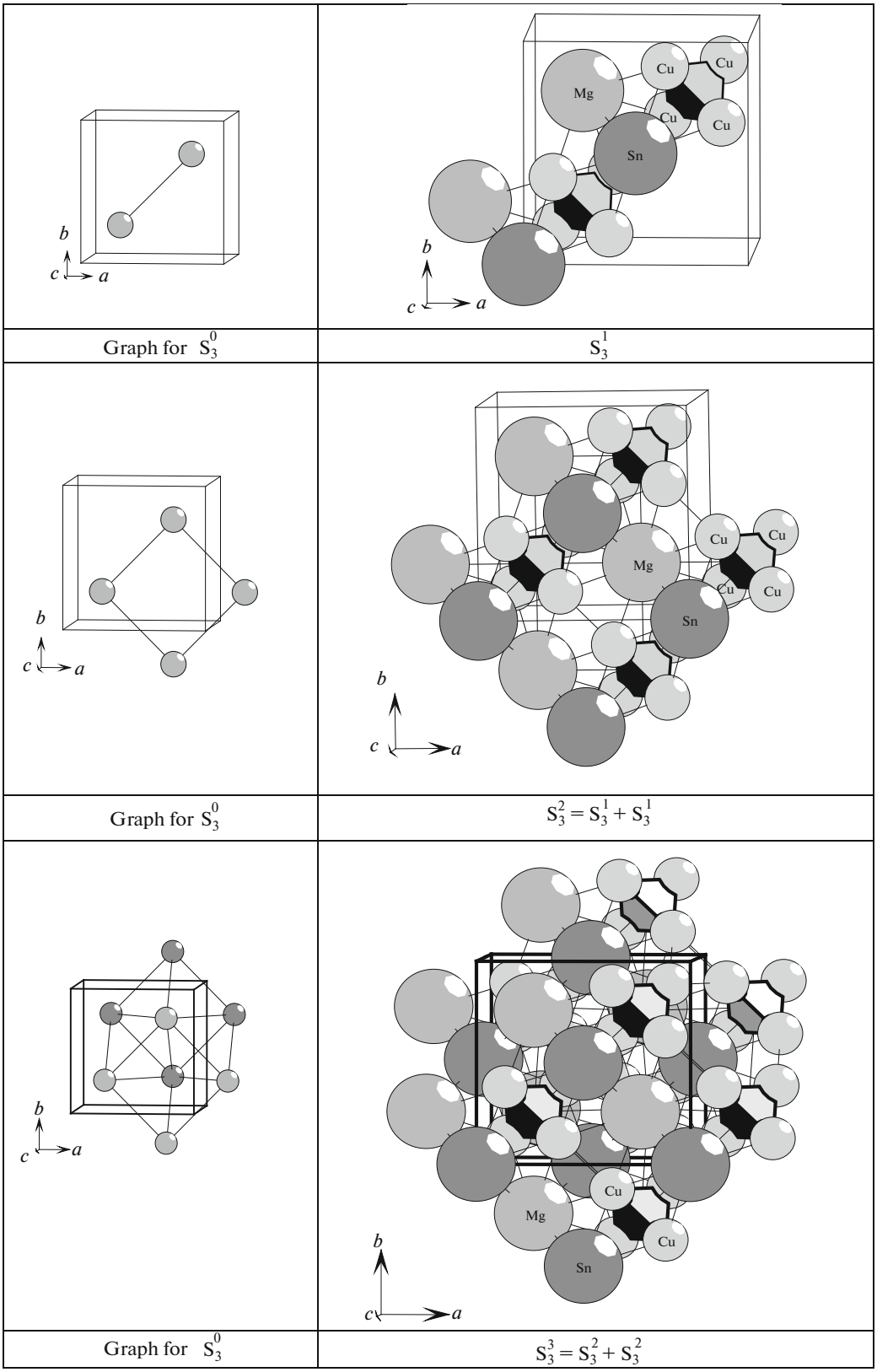

Fig. 16. (Contd.)

4 + 2. The center-to-center distance between tetrahedral clusters corresponds to the translation vector magnitude **c** = 2.941 Å.

Microlayer self-assembly. Microlayer S_3^2 is formed via connection of primary chains in plane *xz* (Fig. 15). The center-to-center distance between clusters Fe_2B_2 from neighboring chains determines the translation vector magnitude **a/2** = 5.495 Å/2.

Microframework self-assembly. Microframework S_3^3 is formed via connection of two microlayers (Fig. 4c). The distance between microlayers corresponds to the translation vector magnitude **c** = 4.048 Å.

Mg_2Cu_4 [40], $(MgSn)Cu_4$ [41], and $(ZrCu)Cu_4$ [42] Crystal Structures

The A_2B_4 stoichiometry was identified for 241 intermetallic compounds. A total of 25 chemically different framework-forming tetrahedral metal clusters B_4 were identified (Fig. 16).

In a unit cell, there are four precursor clusters Mg_2Cu_4, $MgSnCu_4$, or $(ZrCu)Cu_4$ (Fig. 16). The center of the tetrahedral precursor cluster Cu_4 in the $MgSnCu_4$ crystal structure is in the position 4*d* (¼, ¼, ¾) with point symmetry $g = -43m$.

The basal 3D cubic network with CN = 6 and basal 2D network 4^4 (Fig. 16).

Primary chain. Self-assembly of primary chains occurs in the diagonal direction in plane *xy* (Fig. 16) with the connectivity index $P_{loc} = 6$ (equal to the number of bonds: 3 Sn–Cu + 2 Mg–Cu + 1 Cu–Cu). The Sn and Mg atoms lying in between clusters fix their mutual positions in the space. The center-to-center distance between clusters corresponds to a halved diagonal.

Microlayer self-assembly. Microlayer S_3^2 is formed via connection of two parallel lying primary chains in plane *xy* to form Sn–Mg–Sn–Mg chains (Fig. 16). Thereby, the mutual arrangement of two primary chains is fixed in the plane. The center-to-center distances between tetrahedra Cu_4 from neighboring chains in the direction of axis *x* and *y* correspond to the translation vector magnitudes **a** = **b** = 7.042 Å.

Microframework self-assembly. Microframework S_3^3 is formed via connection (with a shift) of two microlayers (Fig. 16). The distance between microlayers determines the halved translation vector magnitude **c** = 7.059 Å.

The size of interstices in a 3D framework built of four connected tetrahedra determines the size of large atoms A. The ratio of atomic radii was fixed at $r_A/r_B = 1.345$, and the ratio of atomic volumes $V_A/V_B = (1.345)^3 = 2.433$.

$MgZn_2$ Structure Type [43]

In a unit cell, there are two precursor clusters Mg_2Zn_4 (Fig. 17). The center of a precursor cluster Zn_4 is in the position 4*e* (0, 0, 0.31) with symmetry $g = 3m$. The basal 3D network is with CN = 6 + 1 + 1 and 2D network 3^6 (Fig. 17).

Primary chain. Self-assembly of primary chains occurs in the direction of axis *x* in plane *xy* (Fig. 17) with the connectivity index $P_{loc} = 6$, equal to the number of bonds: 5 Mg–Zn + 1 Zn–Zn. The Mg atoms are arranged in between clusters Zn_4 and fix the mutual arrangement of clusters Mg_2Zn_4 in the space; that is, the same primary chain assembly mechanism exists in Mg_2Zn_4 and Mg_2Cu_4 ($MgSnCu_4$). The center-to-center distance between clusters Zn_4 corresponds to the translation vector of hexagonal lattice **a** = 5.233 Å.

Microlayer self-assembly. Microlayer S_3^2 is formed in the direction of axis *y* via connection of parallel lying short chains (with a shift) by the identity mechanism of local interactions of clusters Mg_2Zn_4 (Fig. 17). Thereby, the mutual arrangement of two primary chains is fixed in plane *xy* to form Mg–Mg–Mg–Mg chains (Fig. 17); that is, different mechanisms are operated in the assembly of a microlayer from equivalent primary chains in Mg_2Zn_4 and Mg_2Cu_4 ($MgSnCu_4$) crystal structures. The axis-to-axis distance between primary chains (passing through he centers of mass of clusters Zn_4) corresponds to the translation vector of hexagonal lattice **b** = 5.233 Å.

Microframework self-assembly. Microframework S_3^3 is formed via connection of two microlayers (Fig. 17). The distance between microlayers determines a halved translation vector magnitude **c** = 8.566 Å.

The size of interstices in a 3D framework of Mg_2Zn_4 is the same as in Mg_2Cu_4 ($MgSnCu_4$); accordingly, the ratio of atomic radii is fixed at $r_A/r_B = 1.345$.

$(CaCu)Cu_4$ Structure Type [44]

The hexagonal unit cell parameters: $a = b = 5.107$ Å, $c = 4.050$ Å, $V = 91.46$ Å^3, space group *P*6/*mmm* (no. 191).

In a unit cell, there is one precursor cluster Cu_4 (Fig. 18). The center of a precursor cluster Cu_4 is in the position 4*h* (1/3, 2/3, 5/8) with point symmetry $g = 3m$. The basal 3D network with CN = 6 + 1 + 1 and 2D network 3^6 (Fig. 18) is the same as for Mg_2Zn_4.

Primary chain. Self-assembly of primary chains occurs in the direction of axis *x* in plane *xy* (Fig. 18) with the connectivity index $P_{loc} = 6$. The Ca1 and Cu1 atoms are arranged in between clusters Cu_4 and fix the mutual arrangement of clusters $(CaCu)Cu_4$ in the space; that is, the same primary chain assembly mechanism operates as in Mg_2Zn_4 and Mg_2Cu_4 crystal

(a)

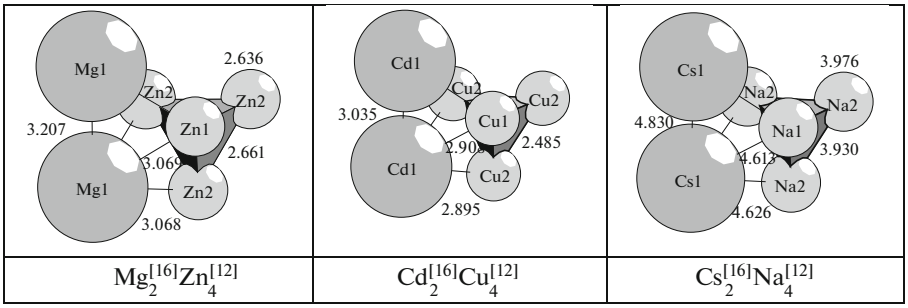

$Mg_2^{[16]}Zn_4^{[12]}$ | $Cd_2^{[16]}Cu_4^{[12]}$ | $Cs_2^{[16]}Na_4^{[12]}$

(b)

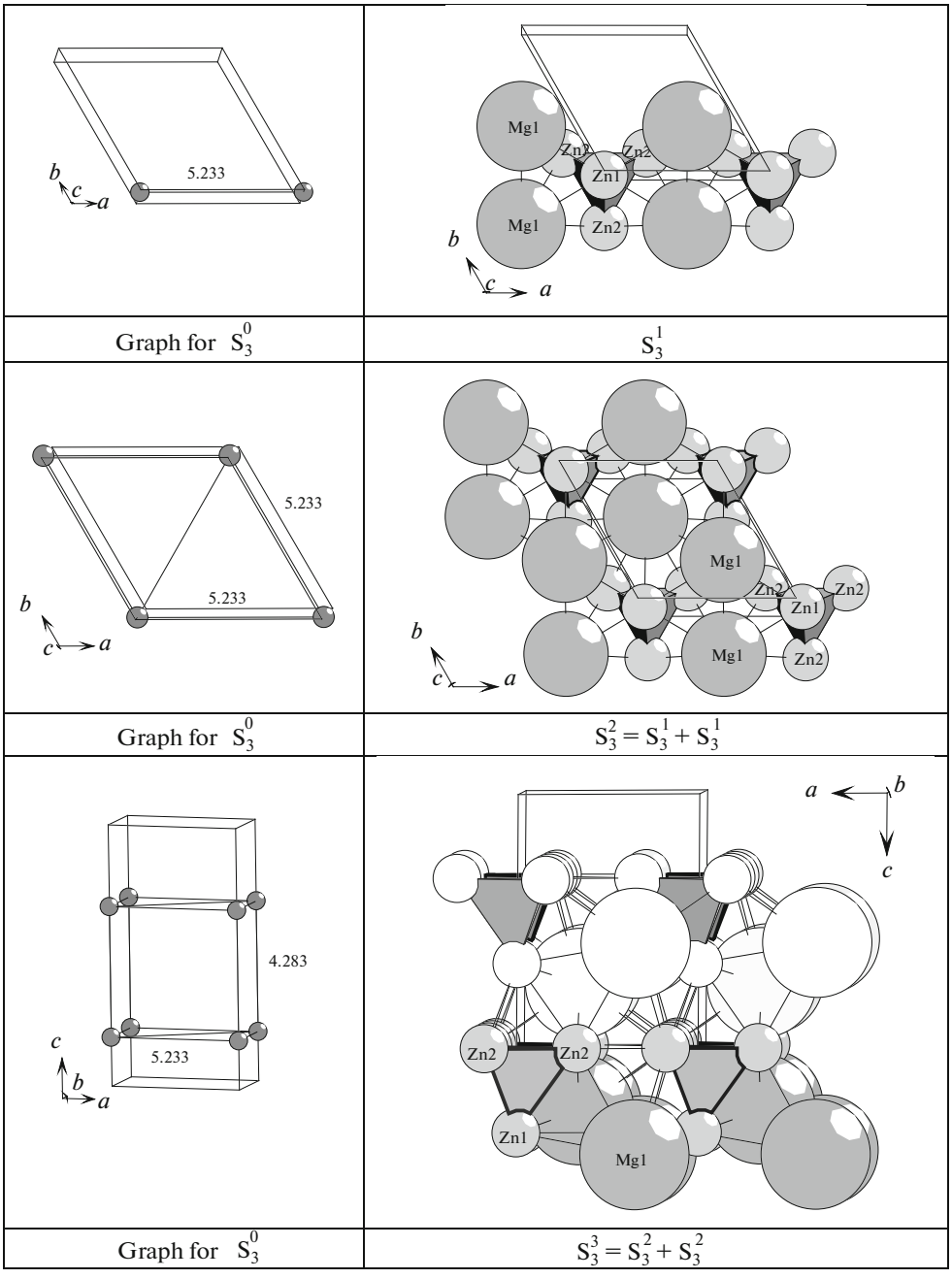

Fig. 17. (a) Precursor clusters. (b) Crystal structure self-assembly stages for $MgZn_2$.

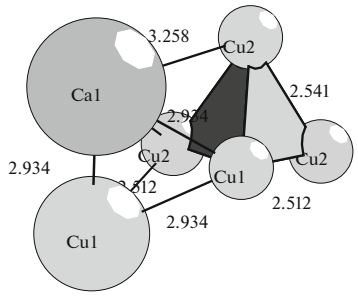

S_3^0

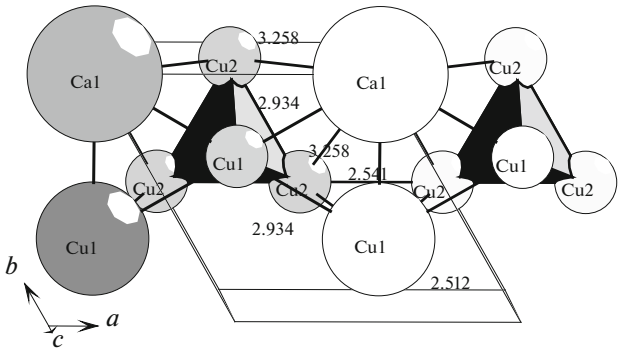

S_3^1

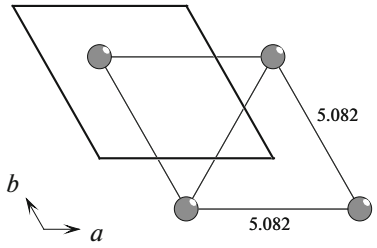

Graph for S_3^0

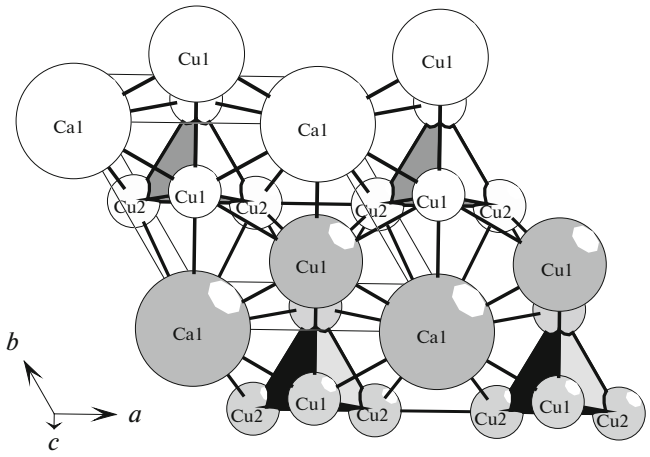

$S_3^2 = S_3^1 + S_3^1$

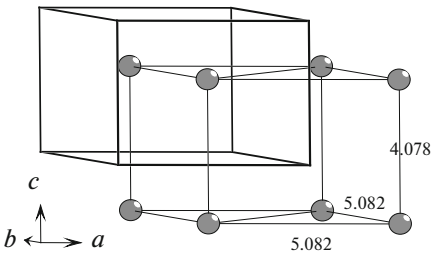

Graph for S_3^0

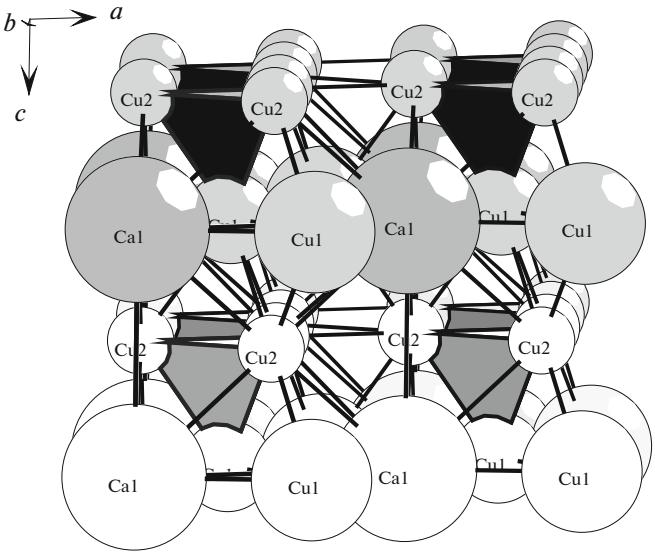

$S_3^3 = S_3^2 + S_3^2$

Fig. 18. $(CaCu)Cu_4$. Crystal structure self-assembly stages.

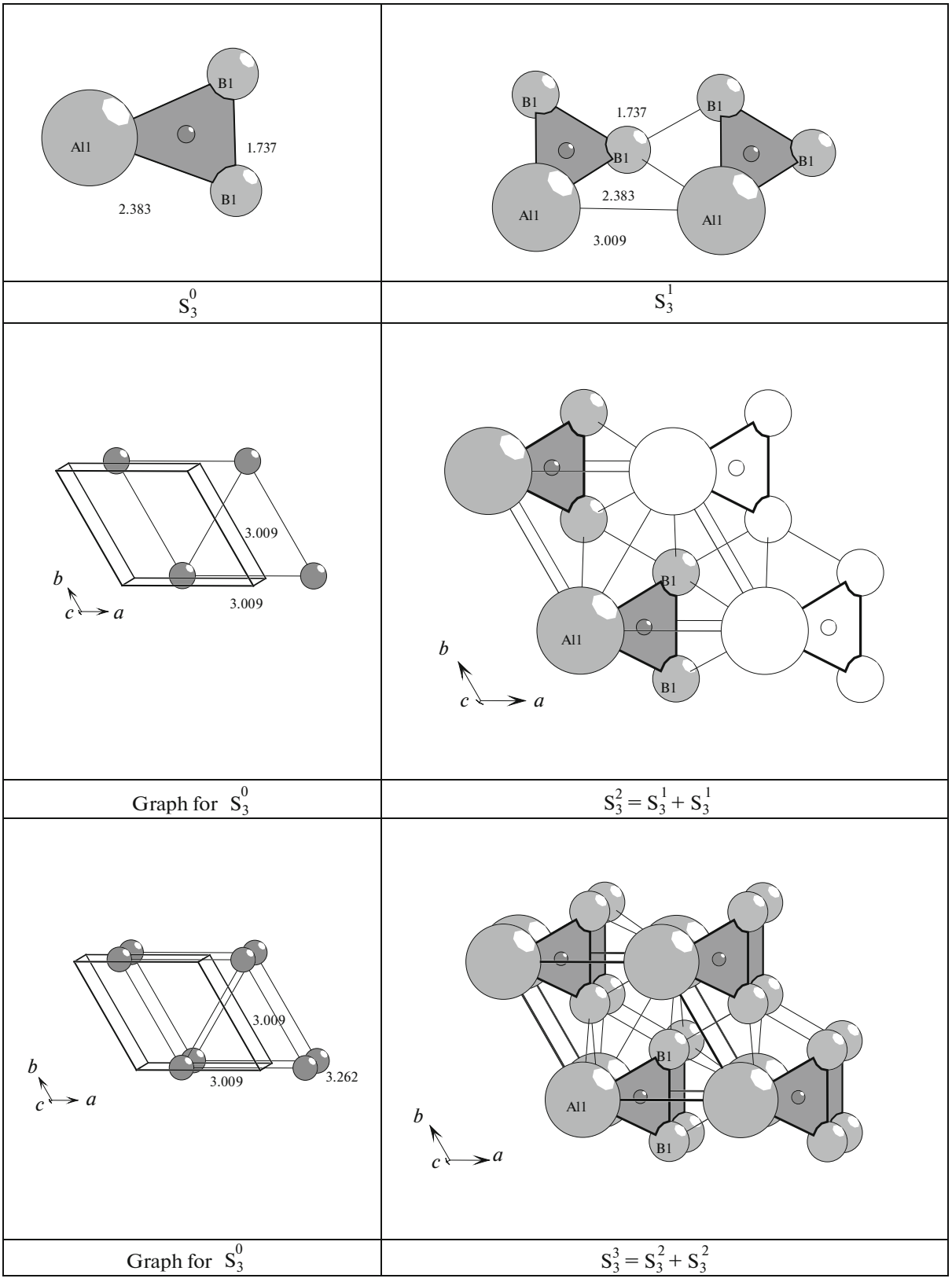

S_3^0	S_3^1
Graph for S_3^0	$S_3^2 = S_3^1 + S_3^1$
Graph for S_3^0	$S_3^3 = S_3^2 + S_3^2$

Fig. 19. AlB_2. Crystal structure self-assembly stages.

structures. The center-to-center distance between clusters Cu_4 corresponds to the translation vector of hexagonal lattice **a** = 5.107 Å.

Microlayer self-assembly. Microlayer S_3^2 is formed in the direction of axis *y* via the connection of parallel lying short chains (with a shift) by the identity mechanism of local interactions of clusters $(CaCu)Cu_4$ (Fig. 18). Thereby, the mutual arrangement of two primary chains is fixed in plane *xy* to form Ca–Cu–Ca–Cu chains in the direction of axis *y* (Fig. 18); that is, there operates the same mechanism of microlayer assembly from primary chains as in Mg_2Zn_4. The axis-to-axis distances between primary chains corresponds to the translation vector of hexagonal lattice **b** = 5.107 Å.

Microframework self-assembly. Microframework S_3^3 is formed via connection of two microlayers (Fig. 18). The distance between microlayers determines the shortest translation vector **c** = 4.050 Å.

AlB_2 Crystal Structure [45]

The hexagonal unit cell parameters are a = 3.009 Å, c = 3.262 Å, V = 25.58 Å^3, Z = 1 AlB_2, space group $P6/mmm$ (no. 191). Point symmetry elements: g = $6/mmm$, $-6m2$, $6mm$, $3m$, etc.

In the unit cell there is one precursor cluster AlB_2 built of three cyclically bonded atoms (Fig. 19). The center of a precursor cluster is in the position 12*n* with symmetry $g = m$. The basal 3D network corresponds to a basal 3D network with CN = 6 + 1 + 1 and 2D network 3^6.

Primary chain. Self-assembly of primary chains from clusters AlB_2 occurs in the direction of axis *x* (Fig. 19) with the connectivity index P_{loc} = 3. The center-to-center distance between clusters AlB_2 determines the translation vector magnitude **a** = 3.009 Å.

Microlayer self-assembly. Microlayer S_3^2 is formed via connection, with a shift, of primary chains in plane *xz*. The distance between primary chains determines the translation vector magnitude **b** = 3.009 Å.

Microframework self-assembly. Microframework S_3^3 is formed via connection of two microlayers (Fig. 19). The distance between primary chains from neighboring microlayers determines the translation vector magnitude **c** = 3.262 Å.

Sc_2Pt Crystal Structure [46]

The orthorhombic unit cell parameters are a = 6.592 Å, b = 4.491 Å, c = 8.206 Å, V = 242.94 Å^3, Z = 4. Space group: $Pnma$ (no. 62). Point symmetry elements: $g = -1$ and m.

In the unit cell there are four precursor cluster Sc_2Pt formed of three cyclically bonded atoms (Fig. 20). The center of a precursor cluster is in the general position 8*d* (0.79, 0.58, 0.72).

Basal 3D network with CN = 6 (4 + 1 + 1) and 2D network of type 4^4.

Primary chain. Self-assembly of primary chains from clusters Sc_2Pt occurs in the direction of axis *x* (Fig. 20) with the connectivity index P_{loc} = 4. The center-to-center distance between clusters determines the translation vector magnitude **a/2** = 6.592/2 Å.

Microlayer self-assembly. Microlayer S_3^2 is formed via connection of primary chains in plane *xz*. The distance between primary chains determines the translation vector magnitude **c/2** = 8.206/2 Å.

Microframework self-assembly. Microframework S_3^3 is formed via connection of two microlayers (Fig. 20). The distance between primary chains from neighboring microlayers determines the translation vector magnitude **b** = 4.491 Å.

$CaHg_2$ Crystal Structure [47]

The hexagonal unit cell parameters are $a = b$ = 4.890 Å, c = 3.564 Å, V = 73.8 Å^3, Z = 1. Space group: $P6/mmm$ (no. 191). Point symmetry elements: g = $6/mmm$, $-6m2$, $6mm$, $3m$, etc.

In the unit cell there is one precursor cluster $CaHg_2$ formed of three cyclically bonded atoms (Fig. 21). The center of a precursor cluster is in the position 12*n* (1/3,0, 2/3) with symmetry $g = m$.

Basal 3D network with CN = 6 + 1 + 1 and 2D network 3^6.

Primary chain. Self-assembly of primary chains from clusters $CaHg_2$ occurs in the direction of axis *z* (Fig. 21) with the connectivity index P_{loc} = 5. The center-to-center distance between clusters determines the translation vector magnitude **c** = 3.564 Å.

Microlayer self-assembly. Microlayer S_3^2 is formed via connection, with a shift, of primary chains in plane *xz* (Fig. 21). The distance between primary chains determines the translation vector magnitude **a** = 4.890 Å.

Microframework self-assembly. Microframework S_3^3 is formed via connection of two microlayers (Fig. 21). The distance between primary chains from neighboring microlayers determines the translation vector magnitude **b** = 4.890 Å.

Co_2Ge Crystal Structure [48]

The hexagonal unit cell parameters are $a = b$ = 3.933 Å, c = 5.014 Å, V = 67.17 8 Å^3, Z = 2. Space group: $P6_3/mmc$ (no. 194). Point symmetry elements: $g = -3m$, $-6m2$, $3m$, etc.

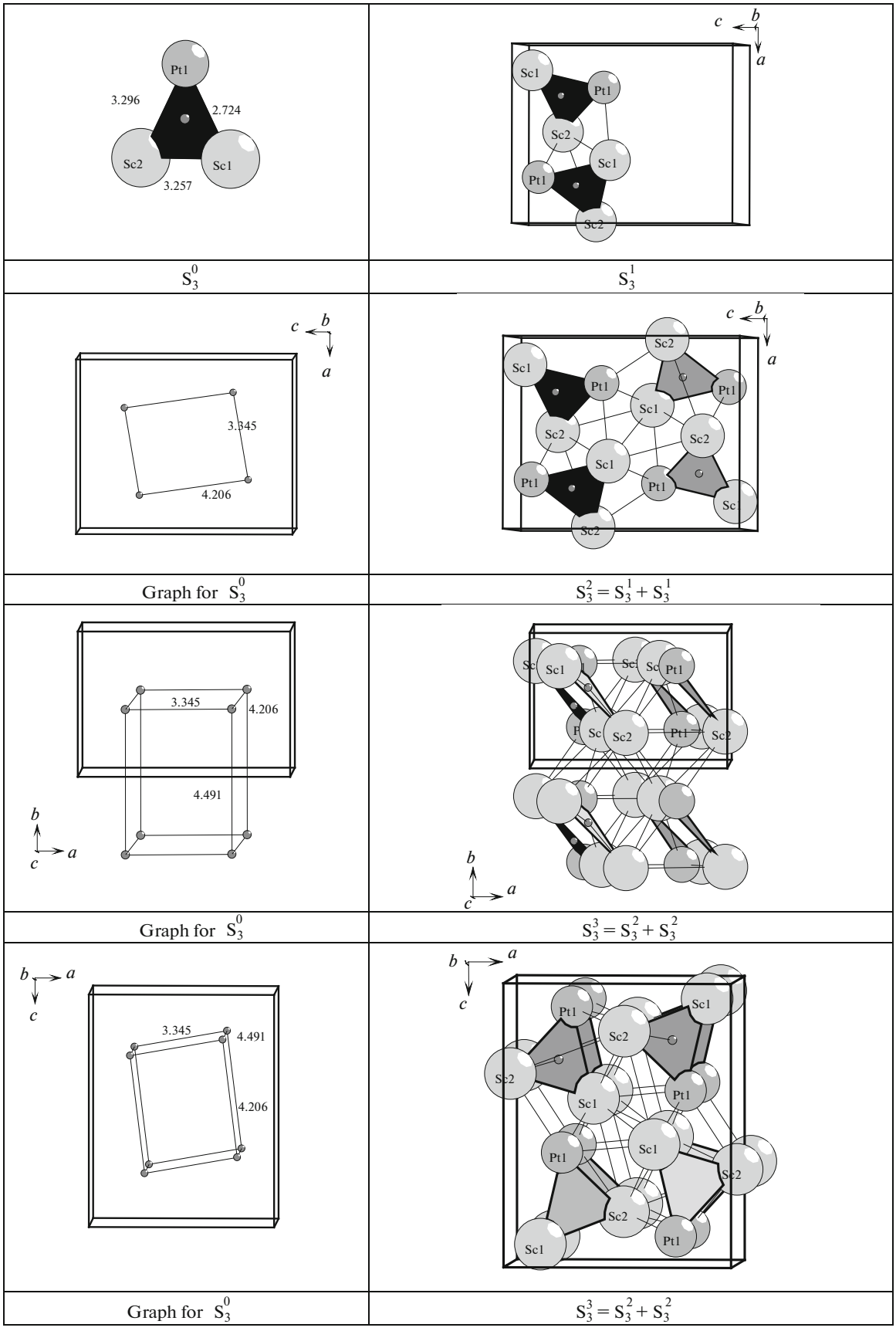

Fig. 20. Sc_2Pt. Crystal structure self-assembly stages.

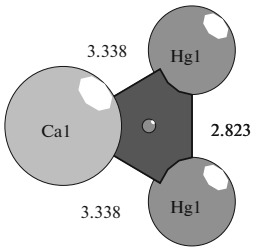

S_3^0

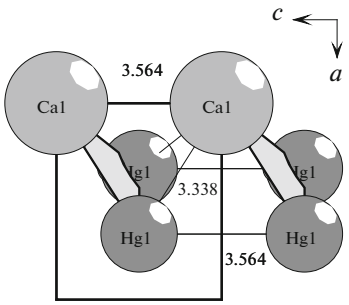

S_3^1

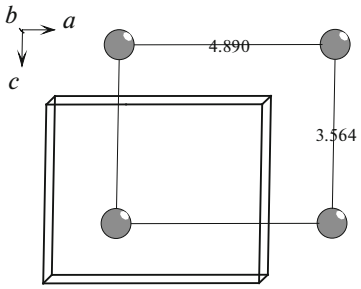

Graph for S_3^0

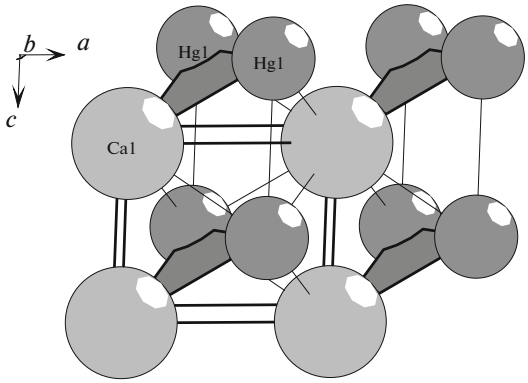

$S_3^2 = S_3^1 + S_3^1$

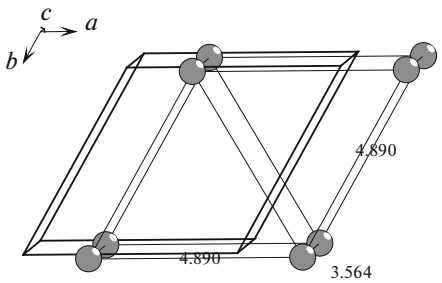

Graph for S_3^0

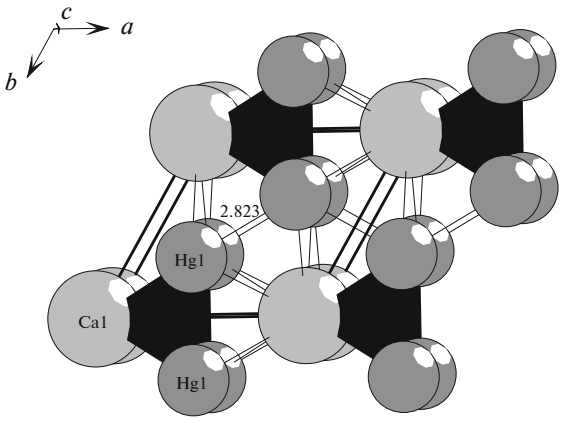

$S_3^3 = S_3^2 + S_3^2$

Fig. 21. $CaHg_2$. Crystal structure self-assembly stages.

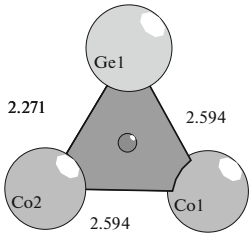

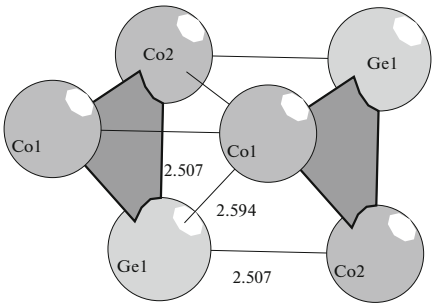

S_3^0 | S_3^1

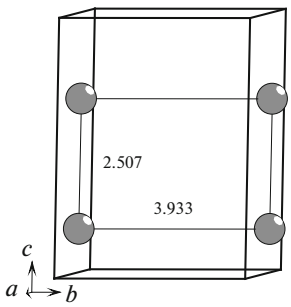

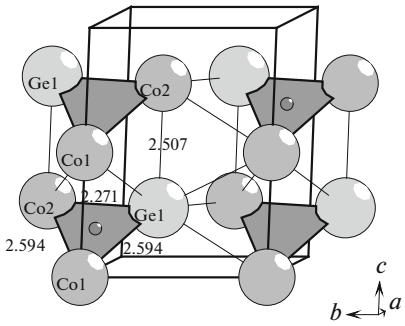

Graph for S_3^0 | $S_3^2 = S_3^1 + S_3^1$

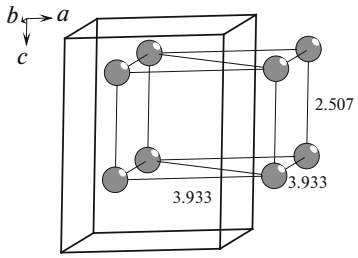

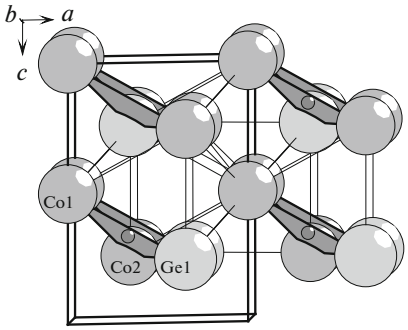

Graph for S_3^0 | $S_3^3 = S_3^2 + S_3^2$

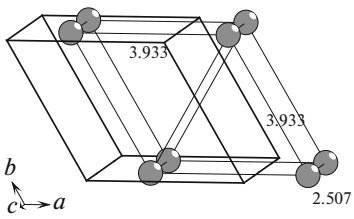

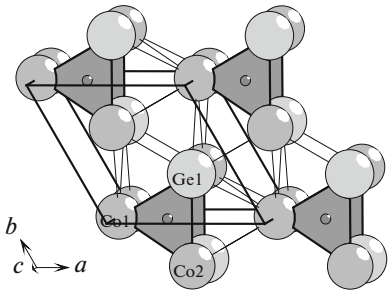

Graph for S_3^0 | $S_3^3 = S_3^2 + S_3^2$

Fig. 22. Co_2Ge. Crystal structure self-assembly stages.

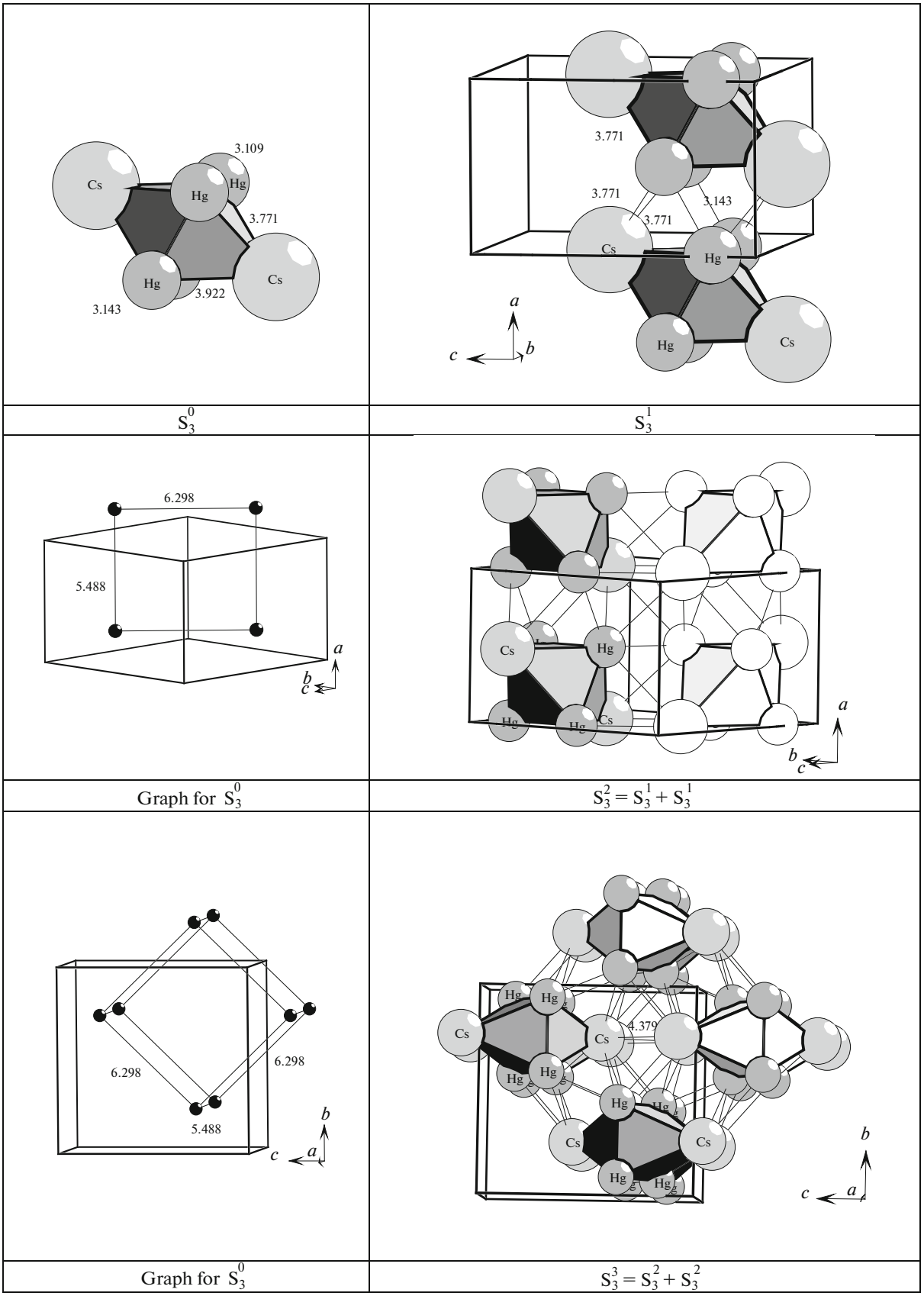

Fig. 23. Cs_2Hg_4. Crystal structure self-assembly stages.

In the unit cell there are two precursor clusters Co_2Ge formed of three cyclically bonded atoms (Fig. 22). The center of a precursor cluster is in the general position 24*l* (1/3, 0, 2/3).

Basal 3D network with CN = 6 + 1 + 1 and 2D network 3^6 .

Primary chain. Self-assembly of primary chains from clusters Co_2Ge occurs in the direction of axis *z* (Fig. 22) with the connectivity index $P_{loc} = 5$. The center-to-center distance between clusters determines the translation vector magnitude **c**/2 = 5.014/2 Å.

Microlayer self-assembly. Microlayer S_3^2 is formed via connection, with a shift, of primary chains in plane *xz*. The distance between primary chains determines the translation vector magnitude **b** = 3.933 Å.

Microframework self-assembly. Microframework S_3^3 is formed via connection of two microlayers (Fig. 22). The distance between primary chains from neighboring microlayers determines the translation vector magnitude **a** = 3.933 Å.

Cs_2Hg_4 Crystal Structure [49]

The orthorhombic unit cell parameters of Cs_2Hg_4: *a* = 5.488 Å, *b* = 8.727 Å, *c* = 9.082 Å, *V* = 434.97 Å^3, *Z* = 2. Space group: *Imma* (no. 74) with the set of elements with point symmetry *g* = 2/*m*, *mm*2, 2, and *m*.

The precursor cluster is an octahedron Cs_2Hg_4. In the unit cell, the center of the cluster is in the position 4*c* with symmetry *g* = 2/*m*. Basal 3D network with CN= 6 (4 + 1 + 1) and basal 2D network 4^4.

Primary chain. Primary chain S_3^1 is formed via connection of precursor clusters Cs_2Hg_4 with the number of bonds equal to the greatest possible value *p* = 6 (Fig. 23). The center-to-center distance between clusters (5.488 Å) corresponds to the translation vector **a**.

Microlayer self-assembly. Microlayer S_3^2 is formed via connection of parallel lying chains in the diagonal direction **b** + **c** (Fig. 23). For connection of primary chains, *p* = 12.

Microframework self-assembly. Microframework S_3^3 is formed via stacking (without shift) of microlayers (Fig. 24). The center-to-center distance between clusters from neighboring chains in the direction of axes *y* and *z* corresponds to translation vectors **b** = 8.727 Å and **c** = 9.082 Å, respectively.

Nd_4Sb_4 (cF8, ba) and Nd_4Sb_4 (tI4, ba) Crystal Structures [50]

The cubic unit cell parameters: *a* = 6.316 Å, *V* = 251.96 Å^3, *Z* = 1, space group *Fm*-3*m* (225). For the low-temperature phase, the tetragonal unit cell parameters [50] are *a* = 4.463 Å, *c* = 6.294 Å, *V* = 125.37 Å^3, *Z* = 1, space group *I*4/*mmm* (139) with point symmetry elements 4/*mmm*, *mmm*, –4*m*2, 4*mm*, etc.

In the unit cell there is one precursor cluster Nd_4Sb_4 in the form of a tetrahedron Nd_4 and four Sb atoms positioned on its faces (Fig. 24). The center of a precursor cluster Nd_4Sb_4 with symmetry *g* = –4*m*2 is in the position 4*d*.

The basal 3D cubic network with CN = 6 and basal 2D network 4^4

Primary chain. Self-assembly of primary chains from clusters Nd_4Sb_4 occurs in the direction of axis *z* (Fig. 24) with the connectivity index $P_{loc} = 4 + 4$. The center-to-center distance between clusters Nd_4Sb_4 determines the translation vector **c** = 6.294 Å.

Microlayer self-assembly. Microlayer $S_3{}^2$ is formed via connection of primary chains in plane (011), *g* = –1, position 4*a* (½, ½, ½). The connectivity index $P_{loc} = 7$ (Fig. 24). The distance between primary chains determines the unit cell diagonal.

Microframework self-assembly. Microframework S_3^3 is formed via connection of two microlayers *g* = –1 (4*b*, ½, ½, 0) (Fig. 24). The distance between microlayers determines the unit cell diagonal.

Mn_5Si_3 (Mavlyanovite) Crystal Structure [51]

The hexagonal unit cell parameters: *a* = 6.897 Å, *c* = 4.807 Å, *V* = 198.05 Å^3, *Z* = 1, space group $P6_3/mcm$ (no. 193).

In the unit cell there is one precursor cluster Mn_6Si_6 in the form of octahedron Mn_6 and six Si atoms arranged on its faces (Fig. 25). The center of a precursor cluster Mn_6Si_6 is in the special position 2*b* with symmetry *g* = –3*m*.

Basal 3D network with CN = 6 + 1 + 1 and 2D network 3^6.

Primary chain. Self-assembly of primary chains from clusters Mn_6Si_6 occurs in the direction of axis *z* (Fig. 25) with the connectivity index $P_{loc} = 12$. The center-to-center distance between clusters Mn_6Si_6 determines the translation vector magnitude **c** = 4.807 Å.

Microlayer self-assembly. Microlayer S_3^2 is formed via connection of primary chains in plane *xz*. The atoms Mn1 are in between primary chains. The distance between primary chains determined the translation vector magnitude **a** = 6.897 Å.

Microframework self-assembly. Microframework S_3^3 is formed via connection of two microlayers with a shift (Fig. 25). The atoms Mn1 are in between primary chains. The distance between primary chains from neighboring microlayers determines the translation vector magnitude **b** = 6.897 Å.

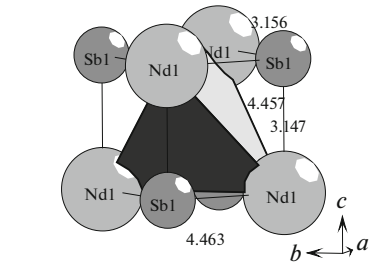

S_3^0

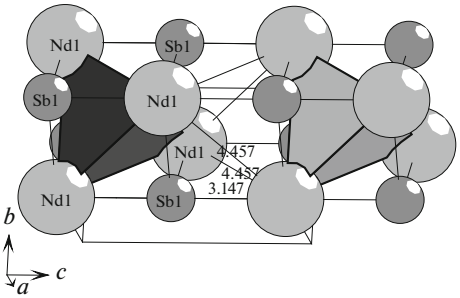

S_3^1

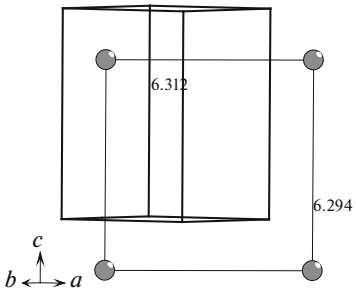

Graph for S_3^0

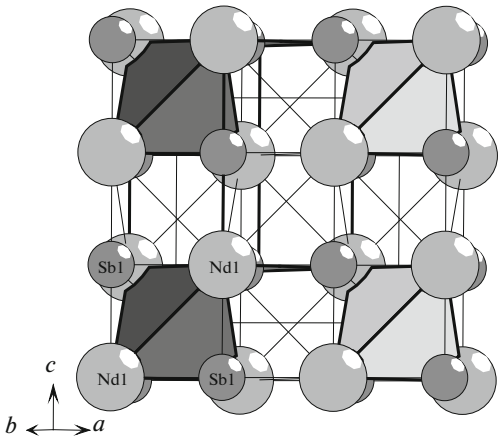

$S_3^2 = S_3^1 + S_3^1$

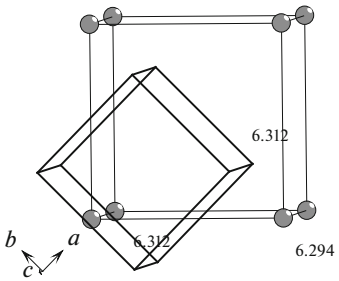

Graph for S_3^0

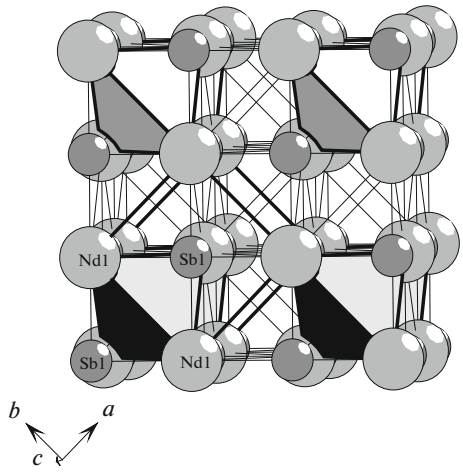

$S_3^3 = S_3^2 + S_3^2$

Fig. 24. Nd_4Sb_4. Crystal structure self-assembly stages.

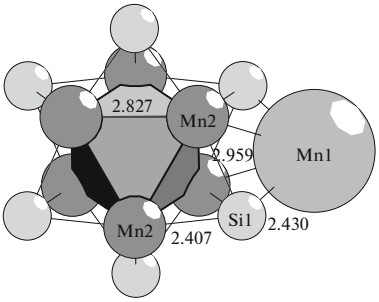

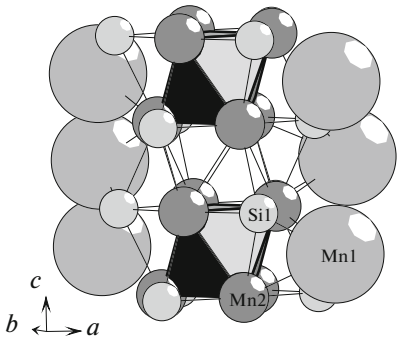

S_3^0 | S_3^1

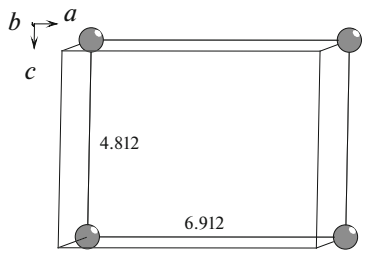

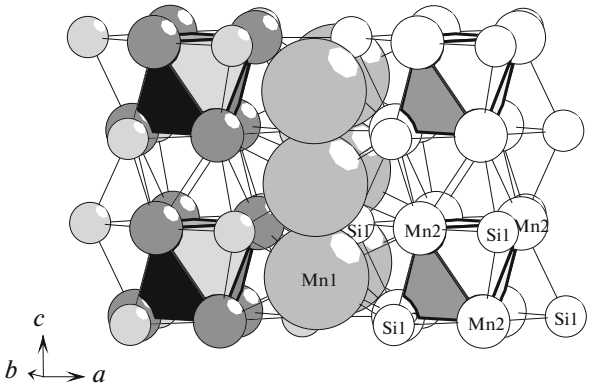

Graph for S_3^0 | $S_3^2 = S_3^1 + S_3^1$

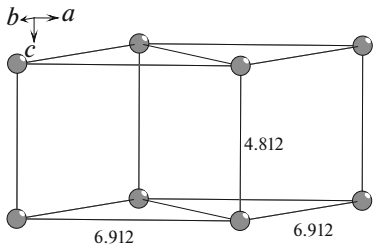

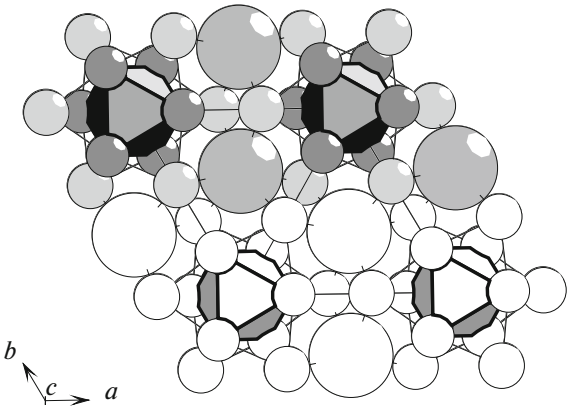

Graph for S_3^0 | $S_3^3 = S_3^2 + S_3^2$

Fig. 25. $Mn_4(Mn_6Si_6)$. Crystal structure self-assembly stages.

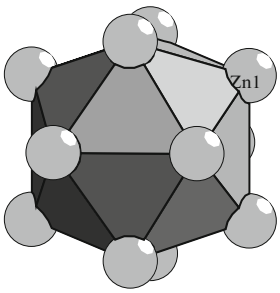

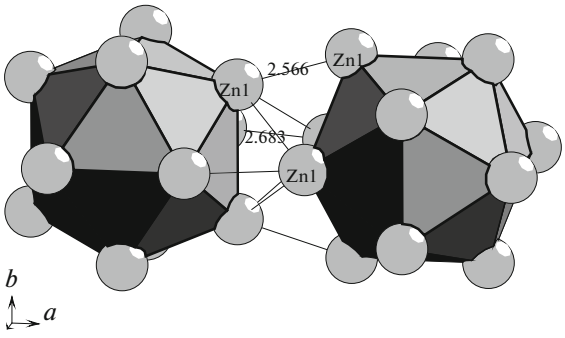

S_3^0 | S_3^1

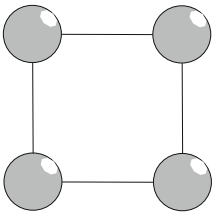

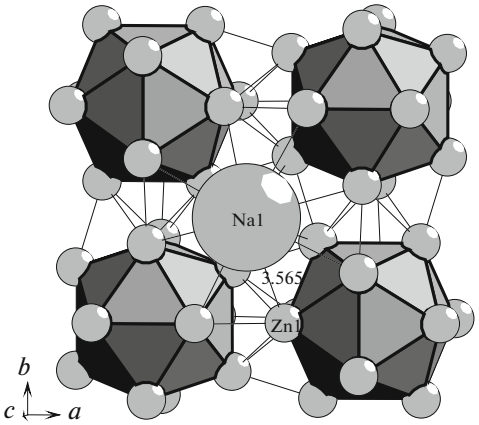

Graph for S_3^0 | $S_3^2 = S_3^1 + S_3^1$

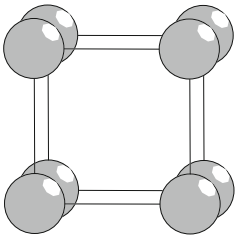

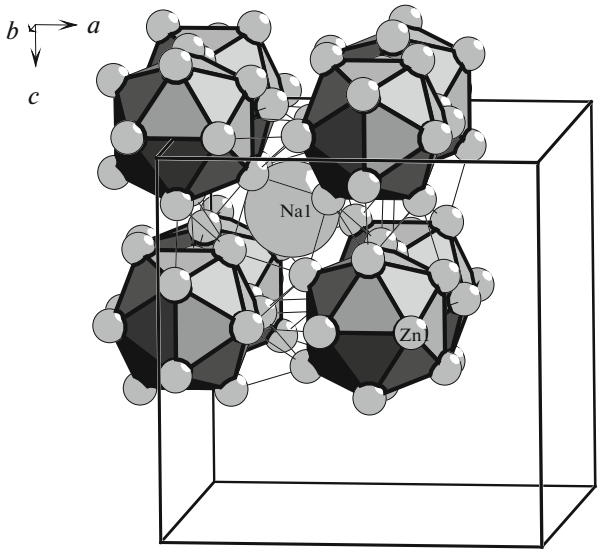

Graph for S_3^0 | $S_3^3 = S_3^2 + S_3^2$

Fig. 26. $NaZn_{13}$. Crystal structure self-assembly stages.

$NaZn_{13}$ Crystal Structure [52]

The cubic unit cell parameters of $NaZn_{13}$: a = 12.273 Å, V = 1848.64 Å^3, Z = 8. The set of elements with high point symmetry: 432, m-3, $-4m.2$, $4/m$ (position 24*d*), etc.

The precursor cluster is an icosahedron built of 12 Zn atoms centered with a Zn atom, which occupies the position 8*b* with the highest possible crystallographic symmetry m-3.

Basal 3D network with CN = 6 (4 + 1 + 1) and basal 2D network 4^4.

Primary chain. The center-to-center distance between clusters (5.488 Å) corresponds to the translation vector **a**.

Self-assembly of primary chains S_3^1 occurs in the direction of axis x (Fig. 26). The supracluster symmetry: $-4m.2$ (position 24*c*). For icosahedra connection, $P_{loc} = 8$.

Microlayer self-assembly. Microlayer S_3^2 is formed via connection of parallel lying short chains S_3^1 (Fig. 26). The center of the supracluster occupies the position 24*d* with symmetry $4/m$. The Na template atoms are positioned above the center of microlayer.

Microframework self-assembly. Microframework S_3^3 is formed by stacking microlayers (Fig. 26). The supracluster center occupies the position occupies the position 8*a* with symmetry 432. The Na atom centers the interstice and forms 24 bonds (three with each of the eight icosahedra). The multiple condensation of the suprapolyhedral cluster built of eight complementarily connected icosahedra gives rise to the self-assembly of 3D macrostructure of $NaZn_{12}$. All interstices are filled with Na atoms. In the framework structures of intermetallic compounds, the geometrical characteristics of polyhedra (Zn–Zn bond lengths in icosahedral shells) and Zn–Zn bond lengths between polyhedra determine the sizes of metal atoms that can fill in these interstices.

In the framework structures of intermetallic compounds, the geometrical characteristics of polyhedra (Zn–Zn bond lengths in an icosahedron) and Zn–Zn bond lengths between polyhedra determine the size of large metal A atoms with CN = 24 that can fill in these interstices. In AZn_{13}-type structures, where small (~5–7 Å) quasi-spherical structural units of icosahedral clusters Be_{13}, Co_{13}, Cu_{13}, Zn_{13}, and Cd_{13} are packed with CN = 6, small interstices in the 3D framework are completely occupied by atoms A. The largest family is ABe_{13}, where A = Hf, Zr, Mg, Dy, Tb, Ce, Th, U, Np, Pu, Ca, Sr, or Ba [14, 15].

CONCLUDING REMARKS

In solving problems in the field of modeling the cluster self-organization of crystal-forming systems where long-range order spontaneously appears in the arrangement of nanolevel structural units that initially existed in a dynamic state as a chaotic mixture, we used the following:

(1) Identification of precursor clusters on the basis of partitioning the structural graph into nonintersecting cluster substructures.

(2) Reconstruction of the algorithm of the most likely mechanism of assembly, from clusters, of a chain, a layer, and a framework in crystal structures. The selection of growing fragments by the criterion of a maximal cluster connectivity index in transition to a higher structural organization level.

These techniques helped us in modeling of various types of crystal structures to determine the sequences of elementary events that lead to the generation of clusters; selection criteria have been formulated for recognizing clusters that are capable of evolving to give rise to a long-range order in three-dimensional periodic structures. The shortest matrix assembly algorithms (programs) have been determined for crystal structures. Frequency analysis of various topology and symmetry pathways of cluster generation and evolution has helped us to establish new crystal-formation laws for chemical systems at the nanolevel.

ACKNOWLEDGMENTS

This study was supported by the Russian Foundation for Basic Research, project no. 16-02-00105, and the Government of the Russian Federation (grant no. 14.B25.31.0005).

The author is grateful to V.A. Blatov for providing the TOPOS 4.0 program package and for fruitful discussion.

REFERENCES

1. G. D. Ilyushin, *Modeling of Self-Organization Processes in Crystal-Forming Systems* (Editorial URSS, Moscow, 2003) [in Russian].
2. W. Pearson, *The Crystal Chemistry and Physics of Metals and Alloys* (Wiley, New York, 1972; Mir, Moscow, 1977).
3. A. I. Kitaigorodskii, *Mixed Crystals* (Nauka, Moscow, 1983) [in Russian].
4. A. F. Wells, *Structural Inorganic Chemistry*, 5th ed. (Oxford Univ. Press. London, 1984).
5. A. A. Pankova, T. G. Akhmetshina, V. A. Blatov, and D. M. Proserpio, Inorg. Chem. **54**, 6616 (2015). http://topospro. com/.
6. A. Pankova, V. Blatov, G. Ilyushin, and D. Proserpio, Inorg. Chem. **52**, 13094 (2013).
7. V. A. Blatov, G. D. Ilyushin, and D. M. Proserpio, Chem. Mater. **25**, 412 (2013).
8. J. L. C. Daams, J. H. N. van Vucht, and P. Villars, J. Alloys Compd. **182**, 1 (1992).
9. J. L. C. Daams and P. Villars, J. Alloys Compd. **215**, 1 (1994).

10. J. Dshemuchadse and W. Steurer, Inorg. Chem. **54**, 1120 (2015).
11. J. Dshemuchadse and W. Steurer, Acta Crystallorg., Sect. A **71**, 335 (2015).
12. V. A. Blatov, Zh. Strukt. Khim. **50**, S166 (2009).
13. V. A. Blatov, A. P. Shevchenko, and D. M. Proserpio, Cryst. Growth Des. **14**, 3576 (2014).
14. *Inorganic Crystal Structure Database (ICSD)* (Fachinformationszentrum, Karlsruhe; US Nat. Inst. Standard and Technology).
15. P. Villars and K. Cenzual, *Pearson's Crystal Data-Crystal Structure Database for Inorganic Compounds* (PCDIC) (ASM Int. Materials Park, OH).
16. G. D. Ilyushin and L. N. Dem'yanets, *The Model for Crystal Structure Matrix Assembly. Physics of Crystallization* (Fizmatlit, Moscow, 2002) [in Russian].
17. G. D. Ilyushin, Russ. J. Inorg. Chem. **61**, 1727 (2016).
18. G. D. Ilyushin, Crystallogr. Repts **49** (7) (2004).
19. G. D. Ilyushin, Struct. Chem. **20**, 975 (2012).
20. G. D. Ilyushin and V. A. Blatov, Acta Crystallogr., Sect. B **65**, 300 (2009).
21. P. Ramdohr, Fortschr. Miner. **28**, 69 (1949).
22. P. Bayliss, Can. Mineral. **28**, 751 (1990).
23. C. H. Johansson and J. O. Linde, Ann. Phys. **5**, 1 (1936).
24. D. A. Edwards, W. E. Wallace, and R. S. Craig, J. Am. Chem. Soc. **74**, 5256 (1952).
25. H. Steeple, Acta Crystallogr. **5**, 247 (1952).
26. W. Hume-Rothery and G. V. Raynor, Proc. R. Soc. London, Ser. A **174**, 471 (1940).
27. E. Zintl and A. Schneider, Z. Elektrochem. Angew. Phys. Chem. **41**, 771 (1935).
28. E. Zintl and G. Brauer, Z. Phys. Chem. B **20**, 245 (1933).
29. W. Hume-Rothery, F. Lewin, and P. W. Reynolds, Proc. R. Soc. London, Ser. A **157**, 167 (1936).
30. E. Zintl and W. Dullenkopf, Z. Phys. Chem. B **16**, 195 (1932).
31. H. Pauly, A. Weiss, and H. Witte, Z. Metallkunde **59**, 47 (1968).
32. L. Lacroix-Orio, M. Tillard, and C. Belin, Solid State Sci. **6**, 1429 (2004).
33. U. Eberz, W. Seelentag, and H. U. Schuster, Z. Naturforsch. **35**, 1341 (1980).
34. Z. Wu, B. D. Mosel, H. Eckert, et al., Chem.-Eur. J. **10**, 1558 (2004).
35. F. Winter, S. Dupke, H. Eckert, et al., Z. Anorg. Allg. Chem. **639**, 2790 (2013).
36. B. Boren, Arkivfoer Kemi, Mineral. Geol., A **11** (1), 1 (1933).
37. F. Givord and R. Lemaire, Solid State Commun. **9**, 341 (1971).
38. S. Okada, T. Atoda, and I. Higashi, J. Solid State Chem. **68**, 61 (1987).
39. C. Kapfenberger, B. Albert, R. Poettgen, and H. Huppertz, Z. Kristallogr. **221**, 477 (2006).
40. J. B. Friauf, J. Am. Chem. Soc. **49**, 3107 (1927).
41. K. Osamura and Y. Murakami, J. Less-Common Met. **60**, 311 (1978).
42. P. Forey, J.-L. Glimois, J.-L. Feron, et al., C. R. Seances Acad. Sci., Ser. C **291**, 177 (1980).
43. J. B. Friauf, J. Am. Chem. Soc. **49**, 3107 (1927).
44. G. Bruzzone, J. Less-Common Met. **25**, 361 (1971).
45. A. Felten, J. Am. Chem. Soc. **78**, 5977 (1956).
46. B. Chabot and E. Parthe, Acta Crystallogr., Sect. B **35**, 1745 (1979).
47. W. Harms, Dissertation (Univ. Freiburg, Breisgau, 2008).
48. F. Laves and H. J. Wallbaum, Z. Angew. Miner. **4**, 17 (1942).
49. H. J. Deiseroth, A. Strunck, and W. Z. Bauhofer, Anorg. Allg. Chem. **558**, 128 (1988).
50. P. Schobinger-Papamantellos and P. Fischer, et al., J. Phys. C **6**, 725 (1973) (ICSD #76738, ICSD #76662).
51. R. G. Yusupov, C. J. Stanley, M. D. Welch, et al., Mineral. Mag. **73**, 43 (2009).
52. M. Wendorff and C. Röhr, J. Alloys Compd. **421**, 24 (2006).

Translated by O. Fedorova